Electronic Supplementary Material (ESI) for Dalton Transactions.
This journal is © The Royal Society of Chemistry 2022

Supporting Information

Schiff Base Tetranuclear Zn2Ln2 Single-Molecule Magnets bridged by Hydroxamic acid in association with Near-Infrared Luminescence

Han Yan, [a] Chu-Meng Wang,[a] Peng Chen,[a] Yi-Quan Zhang,[b] * and Wen-Bin Sun[a]*

a. *Key Laboratory of Functional Inorganic Material Chemistry Ministry of Education, School of Chemistry and Material Science Heilongjiang University, 74 Xuefu Road, Harbin 150080, P. R. China.*

E-mail: wenbinsun@126.com

[b.] Jiangsu Key Laboratory for NSLSCS, School of Physical Science and Technology, Nanjing Normal University, Nanjing 210023, P. R. China.

E-mail: zhangyiquan@njnu.edu.cn

Table S1. Crystallographic data for **1**–**3**.

complex	**1**	**2**	**3**
Empirical formula	$C_{74}H_{72}DY_2F_6N_8O_{22}S_2Zn_2$	$C_{64}H_{62}Dy_2F_6N_6O_{22}S_2Zn_2$	$C_{52}H_{50}Dy_2F_6N_6O_{20}S_2Zn_2$
FW ($g.mol^{-1}$)	2059.25	1901.05	1712.84
Space group	triclinic	triclinic	triclinic
Crystsyst	P-1	P-1	P-1
Temperature (K)	293	293	293
a (Å)	11.4595(8)	11.4657(9)	9.7930(2)
b (Å)	13.0291(9)	12.0293(12)	12.5562(3)
c (Å)	14.9566(13)	13.8868(12)	13.7239(4)
α (°)	66.441(7)	105.941(8)	69.416(2)
β (°)	75.472(7)	106.253(7)	72.247(2)
γ (°)	85.913(6)	90.945(7)	81.336(2)
V ($Å^3$)	1980.5(3)	1759.0(3)	1502.78(7)
ρ_{cacd} ($Mg.m^{-3}$)	1.727	1.795	1.893
μ (mm^{-1})	2.608	2.928	3.413
F(000)	1026.0	942.0	842.0
Independent relections	9053	7448	8045
R_{int}	0.0255	0.0418	0.0400
R_1 [I > 2σ(I)]	0.0248	0.0316	0.0229
wR_2 (all data)	0.0614	0.0798	0.0509
Goodness of fit on F^2	1.053	1.077	1.037
CCDC numbers	2070819	2070820	2070821

Table S2. Crystallographic data for **4**–**6**.

complex	**4**	**5**	**6**
Empirical formula	$C_{56}H_{56}Dy_2F_6N_6O_{20}S_2Zn_2$	$C_{46}H_{54}Dy_2F_6N_6O_{20}S_2Zn_2$	$C_{56}H_{58}Dy_2F_6N_6O_{20}S_2Zn_2$
FW ($g.mol^{-1}$)	1766.92	1644.81	1768.94
Space group	triclinic	triclinic	triclinic
Crystsyst	P-1	P-1	P-1
Temperature (K)	296	296.15	296.15
a (Å)	9.9468(19)	10.0359(8)	12.0729(8)
b (Å)	12.324(2)	12.3262(10)	16.2803(11)
c (Å)	13.388(3)	13.6183(11)	17.2687(11)
α (°)	95.288(2)	107.521(10)	73.557(10)
β (°)	95.851(2)	110.872(10)	88.287(10)
γ (°)	96.332(2)	96.249(10)	78.402(10)
V ($Å^3$)	1613.7(5)	1456.2(2)	3187.6(4)
ρ_{cacd} ($Mg.m^{-3}$)	1.818	1.876	1.843
μ (mm^{-1})	3.181	3.517	3.221
F(000)	872.0	810.0	1748.0
Independent relections	6538	7262	15905
R_{int}	0.0255	0.0209	0.0208
R_1 [I > 2σ(I)]	0.0578	0.0311	0.0319
wR_2 (all data)	0.1732	0.0825	0.0967
Goodness of fit on F^2	1.063	1.048	1.018
CCDC numbers	2070822	2070823	2070824

Table S3. Crystallographic data for **7** and **8**.

complex	**7**	**8**
Empirical formula	$C_{74}H_{74}F_6N_8O_{22}S_2Yb_2Zn_2$	$C_{52}H_{50}F_6N_6O_{20}S_2Yb_2Zn_2$
FW ($g.mol^{-1}$)	2082.35	1733.92
Space group	triclinic	triclinic
Crystsyst	P-1	P-1
Temperature (K)	298	298
a (Å)	11.482(3)	9.6806(15)
b (Å)	13.039(3)	12.528(2)
c (Å)	14.779(4)	13.601(2)
α (°)	66.77(3)	69.687(15)
β (°)	75.78(3)	71.999(14)
γ (°)	85.79(2)	81.437(14)
V ($Å^3$)	1970.3(10)	1469.6(4)
ρ_{cacd} ($Mg.m^{-3}$)	1.755	1.959
μ (mm^{-1})	3.099	4.130
F(000)	1036.0	850.0
Independent relections	8824	7399
R_{int}	0.1133	0.0630
R_1 [I > 2σ(I)]	0.0597	0.0602
wR_2 (all data)	0.1240	0.0922
Goodness of fit on F^2	0.813	0.911
CCDC numbers	2070825	2070827

Table S4. Selected bond lengths (Å) and angles (°) for **1**

Dy1-Dy1′	3.9199(5)	Dy1-O6	2.3033(18)
Dy1-O3	2.3087(17)	Dy1-O1	2.513(2)
Dy1-O7′	2.2830(17)	Dy1-O2	2.3293(17)
Dy1-O7	2.3130(18)	Dy1-O4	2.5452(19)
Dy1-O5	2.335(2)	O7-Dy1′	2.2830(17)
O3-Dy1-Dy1′	104.78(5)	O5-Dy1-Dy1′	170.76(5)
O3-Dy1-O7	77.96(6)	O5-Dy1-O1	88.13(8)
O3-Dy1-O5	84.32(7)	O5-Dy1-O4	90.65(8)
O3-Dy1-O1	129.96(6)	O6-Dy1-Dy1′	98.27(5)
O3-Dy1-O2	66.43(6)	O6-Dy1-O3	137.24(7)
O3-Dy1-O4	63.24(6)	O6-Dy1-O7	129.38(6)
O7-Dy1-Dy1′	31.24(4)	O6-Dy1-O5	73.50(7)
O7′-Dy1-Dy1′	31.70(4)	O6-Dy1-O1	86.13(7)
O7′-Dy1-O3	130.49(7)	O6-Dy1-O2	142.86(7)
O7′-Dy1-O7	62.94(7)	O6-Dy1-O4	80.60(7)
O7-Dy1-O5	157.09(6)	O1-Dy1-Dy1′	87.11(5)
O7′-Dy1-O5	139.60(6)	O1-Dy1-O4	166.46(6)
O7′-Dy1-O6	66.67(6)	O2-Dy1-Dy1′	100.96(4)
O7′-Dy1-O1	82.84(7)	O2-Dy1-O5	83.96(7)
O7-Dy1-O1	92.16(7)	O2-Dy1-O1	63.59(6)
O7-Dy1-O2	75.73(6)	O2-Dy1-O4	129.67(6)
O7′-Dy1-O2	125.17(6)	O4-Dy1-Dy1′	92.12(5)
O7-Dy1-O4	94.18(7)	Dy1′-O7-Dy1	117.06(7)
O7′-Dy1-O4	89.41(7)		

Table S5. Selected bond lengths (Å) and angles (°) for **2**

Dy1-Dy1′	3.9119(6)	Dy1-O7′	2.261(2)
Dy1-O6′	2.312(3)	Dy1-O7	2.324(3)
Dy1-O3	2.321(2)	Dy1-O1	2.520(3)
Dy1-O2	2.321(2)	Dy1-O4	2.548(3)
Dy1-O5	2.339(3)		
O6′-Dy1-Dy1′	99.36(6)	O5-Dy1-O1	89.27(11)
O6′-Dy1-O3	137.33(9)	O5-Dy1-O4	89.72(11)
O6′-Dy1-O2	141.64(10)	O7-Dy1-Dy1′	30.97(6)
O6′-Dy1-O5	75.20(9)	O7′-Dy1-Dy1′	31.93(6)
O6′-Dy1-O7	130.21(9)	O7′-Dy1-O6′	67.52(9)
O6′-Dy1-O1	85.13(9)	O7′-Dy1-O3	129.91(9)
O6′-Dy1-O4	81.35(9)	O7′-Dy1-O2	124.95(9)
O3-Dy1-Dy1′	103.90(7)	O7-Dy1-O5	154.57(9)
O3-Dy1-O2	67.08(8)	O7′-Dy1-O5	142.48(9)
O3-Dy1-O5	81.50(10)	O7′-Dy1-O7	62.91(10)
O3-Dy1-O7	77.31(9)	O7-Dy1-O1	93.72(9)
O3-Dy1-O1	130.21(8)	O7′-Dy1-O1	83.65(9)
O3-Dy1-O4	63.10(8)	O7′-Dy1-O4	88.83(9)
O2-Dy1-Dy1′	100.85(6)	O7-Dy1-O4	93.07(10)
O2-Dy1-O5	82.84(10)	O1-Dy1-Dy1′	88.55(7)
O2-Dy1-O7	76.08(9)	O1-Dy1-O4	166.25(9)
O2-Dy1-O1	63.24(8)	O4-Dy1-Dy1′	91.14(7)
O2-Dy1-O4	130.18(8)	Dy1′-O7-Dy1	117.10(10)
O5-Dy1-Dy1′	174.29(7)		

Table S6. Selected bond lengths (Å) and angles (°) for **3**

Dy1-O2	2.3206(15)	Dy1-O1	2.5351(17)
Dy1-O6’	2.2915(16)	Dy1-O7’	2.2674(16)
Dy1-O3	2.3342(15)	Dy1-O7	2.3141(15)
Dy1-O5	2.3716(17)		
O2-Dy1-O3	67.20(5)	O7’-Dy1-O2	126.61(6)
O2-Dy1-O5	83.44(6)	O7-Dy1-O2	77.54(6)
O2-Dy1-O1	63.07 (5)	O7’-Dy1-O6’	67.18(6)
O6’-Dy1-O2	140.36(6)	O7’-Dy1-O3	129.20(6)
O6’-Dy1-O3	138.03(6)	O7-Dy1-O3	77.06(6)
O6’-Dy1-O5	72.58(6)	O7-Dy1-O5	157.49(6)
O6’-Dy1-O1	84.74(6)	O7’-Dy1-O5	139.56(6)
O6’-Dy1-O7	129.93(6)	O7’-Dy1-O1	84.19(6)
O3-Dy1-O5	84.59(6)	O7-Dy1-O1	93.51(6)
O3-Dy1-O1	130.25(5)	O7’-Dy1-O7	62.88(6)
O5-Dy1-O1	88.43(6)		

Table S7. Selected bond lengths (Å) and angles (°) for **4**

Dy1-Dy1′	3.8968(8)	Dy1-O6	2.308(5)
Dy1-O1′	2.311(5)	O1-Dy1′	2.310(5)
Dy1-O3′	2.322(5)	O3-Dy1′	2.322(5)
Dy1-O3	2.258(5)	O2-Dy1′	2.297(5)
Dy1-O2′	2.297(5)	O4-Dy1′	2.530(5)
Dy1-O4′	2.530(5)		
O1′-Dy1-Dy1′	104.23(12)	O2′-Dy1-Dy1′	101.80(14)
O1′-Dy1-O3′	76.96(17)	O2′-Dy1-O1′	67.52(18)
O1′-Dy1-O4′	63.43(17)	O2′-Dy1-O3′	77.58(19)
O3-Dy1-Dy1′	32.19(12)	O2′-Dy1-O4′	130.95(18)
O3′-Dy1-Dy1′	31.20(11)	O2′-Dy1-O6	140.9(2)
O3-Dy1-O1′	131.01(17)	O4′-Dy1-Dy1′	89.62(13)
O3-Dy1-O3′	63.4(2)	O6-Dy1-Dy1′	98.91(13)
O3-Dy1-O2′	125.04(19)	O6-Dy1-O1′	137.30(19)
O3-Dy1-O4′	88.51(19)	O6-Dy1-O3′	129.88(17)
O3′-Dy1-O4′	90.82(19)	O6-Dy1-O4′	81.6(2)
O3-Dy1-O6	66.93(17)	Dy1-O3-Dy1′	116.6(2)

Table S8. Selected bond lengths (Å) and angles (°) for **5**

Dy1-Dy1’	3.9190(4)	Dy1-O2’	2.327(2)
Dy1-O5’	2.323(2)	Dy1-O7	2.393(3)
Dy1-O5	2.274(2)	Dy1-O3’	2.566(3)
Dy1-O6	2.296(2)	Dy1-O4’	2.535(3)
Dy1-O1’	2.318(2)		
O5’-Dy1-Dy1’	31.15(6)	O6-Dy1-O4’	85.20(10)
O5-Dy1-Dy1’	31.89(6)	O1’-Dy1-Dy1’	102.68(6)
O5-Dy1-O5’	63.05(10)	O1’-Dy1-O5’	77.52(9)
O5-Dy1-O6	67.03(9)	O1’-Dy1-O2’	67.32(9)
O5-Dy1-O1’	126.80(9)	O1’-Dy1-O7	83.00(10)
O5’-Dy1-O2’	77.13(9)	O1’-Dy1-O3’	129.80(9)
O5-Dy1-O2’	129.22(9)	O1’-Dy1-O4’	63.18(9)
O5’-Dy1-O7	157.00(9)	O2’-Dy1-Dy1’	103.59(7)
O5-Dy1-O7	139.88(9)	O2’-Dy1-O7	84.19(9)
O5’-Dy1-O3’	95.41(9)	O2’-Dy1-O3’	62.69(9)
O5-Dy1-O3’	89.94(10)	O2’-Dy1-O4’	130.50(9)
O5’-Dy1-O4’	91.59(9)	O7-Dy1-Dy1’	171.65(7)
O5-Dy1-O4’	82.84(10)	O7-Dy1-O3’	87.70(10)
O6-Dy1-Dy1’	98.88(7)	O7-Dy1-O4’	90.41(10)
O6-Dy1-O5’	129.98(9)	O3’-Dy1-Dy1’	93.17(7)
O6-Dy1-O1’	140.11(10)	O4’-Dy1-Dy1’	86.80(7)
O6-Dy1-O2’	138.13(9)	O4’-Dy1-O3’	166.40(9)
O6-Dy1-O7	73.02(10)	Dy1-O5-Dy1’	116.95(10)
O6-Dy1-O3’	81.36(9)		

Table S9. Selected bond lengths (Å) and angles (°) for **6**

Dy1-Dy1’	3.8755(3)	Dy1-O6	2.316(2)
Dy1-O5	2.272(2)	Dy1-O4’	2.510(2)
Dy1-O5’	2.316(2)	Dy1-O3’	2.484(2)
Dy1-O1’	2.325(2)	Dy1-O7	2.380(2)
Dy1-O2’	2.332(2)	O5-Dy1’	2.321(3)
O5’-Dy1-Dy1’	32.02(5)	O2’-Dy1-Dy1’	103.54(5)
O5-Dy1-Dy1’	32.72(5)	O2’-Dy1-O4’	132.03(8)
O5-Dy1-O5’	64.75(9)	O2’-Dy1-O3’	65.54(8)
O5-Dy1-O1’	122.48(8)	O2’-Dy1-O7	83.46(9)
O5’-Dy1-O1’	76.66(8)	O6-Dy1-Dy1’	99.14 (6)
O5-Dy1-O2’	131.88(8)	O6-Dy1-O5’	130.50(8)
O5’-Dy1-O2’	74.74(8)	O6-Dy1-O1’	142.23(9)
O5-Dy1-O6	66.98(8)	O6-Dy1-O2’	136.86(8)
O5-Dy1-O4’	82.40(9)	O6-Dy1-O4’	82.36(9)
O5’-Dy1-O4’	101.37(8)	O6-Dy1-O3’	78.63(9)
O5-Dy1-O3’	88.95(9)	O6-Dy1-O7	73.82(8)
O5’-Dy1-O3’	90.08(9)	O4’-Dy1-Dy1’	92.31(6)
O5-Dy1-O7	139.93(8)	O3’-Dy1-Dy1’	89.43(6)
O5’-Dy1-O7	155.30(8)	O3’-Dy1-O4’	160.95(8)
O1’-Dy1-Dy1’	100.19(6)	O7-Dy1-Dy1’	172.60(6)
O1’-Dy1-O2’	67.95(8)	O7-Dy1-O4’	84.56(9)
O1’-Dy1-O4’	64.76(8)	O7-Dy1-O3’	91.37(9)
O1’-Dy1-O3’	133.47(8)	Dy1-O5-Dy1’	115.25(9)
O1’-Dy1-O7	84.56(9)		

Table S10. Selected bond lengths (Å) and angles (°) for **7**

Yb1-Yb1’	3.8856(18)	Yb1-O5	2.242(5)
Yb1-O2’	2.257(5)	Yb1-O7	2.283(6)
Yb1-O6	2.236(5)	Yb1-O3’	2.480(5)
Yb1-O1’	2.256(5)	Yb1-O4’	2.508(5)
Yb1-O5’	2.303(6)		
O2’-Yb1-Yb1’	101.20(15)	O5’-Yb1-Yb1’	30.79(13)
O2’-Yb1-O5’	76.4(2)	O1’-Yb1-O4’	62.63(17)
O2’-Yb1-O7	82.7(2)	O5-Yb1-Yb1’	31.71(15)
O2’-Yb1-O3’	64.62(18)	O5-Yb1-O2’	125.3(2)
O2’-Yb1-O4’	129.99(17)	O5-Yb1-O1’	130.6(2)
O6-Yb1-Yb1’	99.71(14)	O5-Yb1-O5’	62.5(2)
O6-Yb1-O2’	141.9(2)	O5-Yb1-O7	141.0(2)
O6-Yb1-O1’	135.5(2)	O5’-Yb1-O3’	93.1(2)
O6-Yb1-O5	68.1(2)	O5-Yb1-O3’	83.32(19)
O6-Yb1-O5’	130.36(19)	O5’-Yb1-O4’	94.7(2)
O6-Yb1-O7	73.43(19)	O5-Yb1-O4’	89.77(18)
O6-Yb1-O3’	85.0(2)	O7-Yb1-Yb1’	172.17(14)
O6-Yb1-O4’	80.09(18)	O7-Yb1-O5’	156.20(19)
O1’-Yb1-Yb1’	105.18(16)	O7-Yb1-O3’	88.2(2)
O1’-Yb1-O2’	67.37(18)	O7-Yb1-O4’	89.9(2)
O1’-Yb1-O5’	78.9(2)	O3’-Yb1-Yb1’	87.41(16)
O1’-Yb1-O7	82.6(2)	O3’-Yb1-O4’	164.84(18)
O1’-Yb1-O3’	131.86(18)	O4’-Yb1-Yb1’	92.66(15)

Table S11. Selected bond lengths (Å) and angles (°) for **8**

Yb1-Yb1’	3.8139(9)	Yb1-O3’	2.501(5)
Yb1-O2’	2.268(5)	Yb1-O7	2.301(4)
Yb1-O5’	2.258(4)	O2-Yb1’	2.268(5)
Yb1-O5	2.217(4)	O5-Yb1’	2.258(4)
Yb1-O1’	2.267(5)	O1-Yb1’	2.267(5)
Yb1-O4’	2.482(5)	O4-Yb1’	2.482(5)
Yb1-O6	2.236(5)	O3-Yb1’	2.501(5)
O2’-Yb1-Yb1’	104.34(11)	O1’-Yb1-O2’	67.84(18)
O2’-Yb1-O4’	131.56(18)	O1’-Yb1-O4’	63.78(17)
O2’-Yb1-O3’	63.51(18)	O1’-Yb1-O3’	131.31(17)
O2’-Yb1-O7	82.89(16)	O1’-Yb1-O7	82.46(18)
O5-Yb1-Yb1’	31.87(11)	O4’-Yb1-Yb1’	89.07(10)
O5’-Yb1-Yb1’	31.22(12)	O4’-Yb1-O3’	164.37(17)
O5’-Yb1-O2’	77.98(15)	O6-Yb1-Yb1’	99.66(11)
O5-Yb1-O2’	129.66(17)	O6-Yb1-O2’	137.40(17)
O5-Yb1-O5’	63.1(2)	O6-Yb1-O5’	130.85(16)
O5’-Yb1-O1’	78.06(17)	O6-Yb1-O1’	138.66(18)
O5-Yb1-O1’	127.30(17)	O6-Yb1-O4’	82.87(19)
O5’-Yb1-O4’	94.19(17)	O6-Yb1-O3’	81.80(18)
O5-Yb1-O4’	84.12(18)	O6-Yb1-O7	72.48(18)
O5-Yb1-O6	67.82(16)	O3’-Yb1-Yb1’	90.52(10)
O5’-Yb1-O3’	93.53(17)	O7-Yb1-Yb1’	172.01(13)
O5-Yb1-O3’	87.30(18)	O7-Yb1-O4’	88.54(17)
O5-Yb1-O7	140.20(17)	O7-Yb1-O3’	89.73(17)
O5’-Yb1-O7	156.67(18)	Yb1-O5-Yb1’	116.9(2)
O1’-Yb1-Yb1’	103.28(10)		

Table S12. Continuous Shape Measures (CShMs) of the coordination geometry for Dy(III) ion in compounds **1**–**8** (S values calculated with the Shape program). The S values indicated the proximity to the ideal polyhedron, thus, *S* = 0 corresponds to the non-distorted polyhedron. The three closer ideal geometries to the real complexes are listed and below are the symmetry and description for each polyhedron.

Complex **1**	Dy1	2.867	TDD-8	6	D2d	Triangular dodecahedron
		3.966	BTPR-8	10	C2v	Biaugmented trigonal prism
		4.790	JSD-8	11	D2d	Snub diphenoid J84
	Dy1’	2.867	TDD-8	6	D2d	Triangular dodecahedron
		3.966	BTPR-8	10	C2v	Biaugmented trigonal prism
		4.790	JSD-8	11	D2d	Snub diphenoid J84
Complex **2**	Dy1	2.617	TDD-8	6	D2d	Triangular dodecahedron
		4.568	JBTPR-8	9	C2v	Biaugmented trigonal prism J50
		3.707	BTPR-8	10	D2d	Biaugmented trigonal prism
	Dy1’	2.617	TDD-8	6	D2d	Triangular dodecahedron
		4.568	JBTPR-8	9	C2v	Biaugmented trigonal prism J50
		3.707	BTPR-8	10	D2d	Biaugmented trigonal prism
Complex **3**	Dy1	2.842	TDD-8	6	D2d	Triangular dodecahedron
		4.893	JBTPR-8	9	C2v	Biaugmented trigonal prism J50
		3.960	BTPR-8	10	D2d	Biaugmented trigonal prism
	Dy1’	2.842	TDD-8	6	D2d	Triangular dodecahedron
		4.893	JBTPR-8	9	C2v	Biaugmented trigonal prism J50
		3.960	BTPR-8	10	D2d	Biaugmented trigonal prism
Complex **4**	Dy1	2.652	TDD-8	6	D2d	Triangular dodecahedron
		4.425	JBTPR-8	9	C2v	Biaugmented trigonal prism J50
		3.511	BTPR-8	10	D2d	Biaugmented trigonal prism
	Dy1’	2.652	TDD-8	6	D2d	Triangular dodecahedron
		4.425	JBTPR-8	9	C2v	Biaugmented trigonal prism J50
		3.511	BTPR-8	10	D2d	Biaugmented trigonal prism
Complex **5**	Dy1	2.866	TDD-8	6	D2d	Triangular dodecahedron
		4.936	JBTPR-8	9	C2v	Biaugmented trigonal prism J50
		3.900	BTPR-8	10	D2d	Biaugmented trigonal prism
	Dy1’	2.866	TDD-8	6	D2d	Triangular dodecahedron
		4.937	JBTPR-8	9	C2v	Biaugmented trigonal prism J50
		3.900	BTPR-8	10	D2d	Biaugmented trigonal prism
Complex **6**	Dy1	2.491	TDD-8	6	D2d	Triangular dodecahedron
		3.583	JBTPR-8	9	C2v	Biaugmented trigonal prism J50
		2.658	BTPR-8	10	D2d	Biaugmented trigonal prism
	Dy1’	2.491	TDD-8	6	D2d	Triangular dodecahedron
		3.583	JBTPR-8	9	C2v	Biaugmented trigonal prism J50
		2.658	BTPR-8	10	D2d	Biaugmented trigonal prism
Complex **7**	Yb1	2.651	TDD-8	6	D2d	Triangular dodecahedron
		4.750	JBTPR-8	9	C2v	Biaugmented trigonal prism J50
		3.768	BTPR-8	10	D2d	Biaugmented trigonal prism
	Yb1’	2.651	TDD-8	6	D2d	Triangular dodecahedron

		4.750	JBTPR-8	9	C2v	Biaugmented trigonal prism J50
		3.768	BTPR-8	10	D2d	Biaugmented trigonal prism
Complex **8**	Yb1	2.506	TDD-8	6	D2d	Triangular dodecahedron
		4.660	JBTPR-8	9	C2v	Biaugmented trigonal prism J50
		3.683	BTPR-8	10	D2d	Biaugmented trigonal prism
	Yb1'	2.506	TDD-8	6	D2d	Triangular dodecahedron
		4.660	JBTPR-8	9	C2v	Biaugmented trigonal prism J50
		3.683	BTPR-8	10	D2d	Biaugmented trigonal prism

Table S13. Best fitted parameters (χ_T, χ_S, τ and α) with the extended Debye model for compound **1** under 0 Oe in the temperature range 2–9.5 K.

T/ K	χ_S / cm^3 mol^{-1}	χ_T / cm^3 mol^{-1}	τ/s	α	R
2	5.84987	9.86892	0.00366	0.30000	7.82×10^{-4}
2.5	5.28413	8.37000	0.00335	0.30000	6.16×10^{-4}
3	4.90000	7.40000	0.00326	0.27784	6.78×10^{-4}
3.5	4.40002	6.71220	0.00298	0.28922	5.83×10^{-4}
4	3.90000	6.10490	0.00242	0.30000	4.00×10^{-4}
4.5	3.53882	5.59617	0.00200	0.29973	2.85×10^{-4}
5	3.35000	5.13741	0.00179	0.25909	2.44×10^{-4}
5.5	3.22086	4.75035	0.00162	0.19678	2.90×10^{-4}
6	2.80976	4.44778	0.00113	0.26674	5.77×10^{-4}
6.5	2.54415	4.14324	0.00082	0.28193	2.59×10^{-4}
7	2.44250	3.88891	0.00068	0.25440	3.15×10^{-4}
7.5	2.30636	3.67088	0.00056	0.24764	5.17×10^{-5}
8	2.13317	3.50049	0.00046	0.29093	9.44×10^{-5}
8.5	2.15601	3.29499	0.00044	0.23203	7.76×10^{-5}
9	1.97766	3.13108	0.00033	0.26334	8.57×10^{-5}
9.5	1.85723	3.00089	0.00027	0.29782	9.78×10^{-5}

Table S14. Best fitted parameters (χ_T, χ_S, τ and α) with the extended Debye model for compound **2** under 0 Oe in the temperature range 2–11K.

T/ K	χ_S / cm^3 mol^{-1}	χ_T / cm^3 mol^{-1}	τ/s	α	R
2	7.81179	8.61841	0.01047	0.29982	1.56×10^{-4}
3	5.85000	6.65015	0.01500	0.29990	1.54×10^{-4}
4	4.67799	5.30000	0.00974	0.30000	1.28×10^{-4}
5	3.87372	4.40121	0.00575	0.27658	1.31×10^{-4}
6	3.30793	3.78522	0.00363	0.27477	1.54×10^{-4}
7	2.89154	3.29376	0.00230	0.23742	1.68×10^{-4}
8	2.59427	2.91290	0.00152	0.16754	2.07×10^{-4}
9	2.34072	2.62104	0.00103	0.15740	2.18×10^{-4}
10	2.19199	2.38019	0.00100	0.07319	2.29×10^{-4}
11	1.99880	2.18395	0.00065	0.16011	2.15×10^{-4}

Table S15. Best fitted parameters (χ_T, χ_S, τ and α) with the extended Debye model for compound **3** under 0 Oe in the temperature range 2–7 K.

T/ K	χ_S / cm^3 mol^{-1}	χ_T / cm^3 mol^{-1}	τ/s	α	R
2	1.09661	7.70000	0.00027	0.12955	1.02×10^{-4}
2.5	0.62992	7.10236	0.00025	0.14708	8.87×10^{-5}
3	1.29720	6.47445	0.00030	0.08278	3.74×10^{-5}
3.5	0.92957	5.92082	0.00028	0.10413	1.96×10^{-5}
4	0.79121	5.42496	0.00027	0.10357	3.13×10^{-5}
4.5	0.80063	5.00164	0.00026	0.09093	2.32×10^{-5}
5	0.95616	4.62177	0.00026	0.05646	1.20×10^{-5}
5.5	0.80902	4.30305	0.00023	0.05085	2.83×10^{-5}
6	0.84285	4.01162	0.00020	0.02719	2.11×10^{-5}
6.5	1.08011	3.76826	0.00020	0.00005	5.65×10^{-5}
7	0.90284	3.53849	0.00016	0.00069	2.50×10^{-5}

Table S16. Best fitted parameters (χ_T, χ_S, τ and α) with the extended Debye model for compound **4** under 0 Oe in the temperature range 2–7 K.

T/ K	χ_S / cm^3 mol^{-1}	χ_T / cm^3 mol^{-1}	τ/s	α	R
2	0.11386	6.10677	0.01210	0.22072	4.34×10^{-4}
2.5	0.14213	5.64939	0.01100	0.20741	4.34×10^{-4}
3	0.15494	5.16657	0.00958	0.19244	4.34×10^{-4}
3.5	0.03000	4.64991	0.00753	0.19211	4.34×10^{-4}
4	0.09436	4.29950	0.00638	0.17040	4.34×10^{-4}
4.5	0.08425	3.98375	0.13099	0.16479	4.34×10^{-4}
5	0.08316	3.68758	0.00403	0.15296	4.34×10^{-4}
5.5	0.07213	3.42829	0.00314	0.14373	4.34×10^{-4}
6	0.07095	3.19632	0.00245	0.13407	4.34×10^{-4}
6.5	0.05670	2.99631	0.00191	0.13252	4.34×10^{-4}
7	0.11390	2.82557	0.00156	0.11474	4.34×10^{-4}
7.5	0.11900	2.66408	0.00125	0.10838	4.34×10^{-4}
8	0.01598	2.52742	0.00097	0.13446	4.34×10^{-4}
8.5	0.00596	2.39752	0.00078	0.13383	4.34×10^{-4}
9	0.25025	2.29944	0.00056	0.20274	4.34×10^{-4}
9.5	0.01110	2.17904	0.00053	0.13567	4.34×10^{-4}
10	0.04206	2.08103	0.00045	0.12309	4.34×10^{-4}
10.5	0.04973	1.99264	0.00038	0.12224	4.34×10^{-4}
11	0.04610	1.91847	0.00032	0.12799	4.34×10^{-4}
11.5	0.05000	1.84432	0.00027	0.12397	4.34×10^{-4}
12	0.06420	1.77856	0.00020	0.15856	4.34×10^{-4}

Table S17. Best fitted parameters (χ_T, χ_S, τ and α) with the extended Debye model for compound **5** under 0 Oe in the temperature range 2–12 K.

T/ K	χ_S / cm^3 mol^{-1}	χ_T / cm^3 mol^{-1}	τ/s	α	R
2	0.25465	3.64831	0.00207	0.17448	1.68×10^{-4}
2.5	0.2537	3.40059	0.00212	0.17366	2.63×10^{-4}
3	0.16347	3.04053	0.00189	0.17851	3.59×10^{-4}
3.5	0.20318	2.80232	0.00177	0.15593	1.85×10^{-4}
4	0.16162	2.60179	0.00158	0.1552	3.42×10^{-4}
4.5	0.22884	2.39573	0.00145	0.11603	2.98×10^{-4}
5	0.22249	2.19841	0.00124	0.10674	3.36×10^{-4}
5.5	0.19837	2.01482	0.00102	0.10355	3.87×10^{-4}
6	0.16546	1.85644	0.00081	0.09627	4.12×10^{-4}
6.5	0.18983	1.74675	0.00068	0.08629	3.49×10^{-4}
7	0.18776	1.6409	0.00056	0.08395	3.95×10^{-4}
7.5	0.17979	1.54762	0.00046	0.08818	4.64×10^{-4}
8	0.18951	1.46776	0.00039	0.09152	4.61×10^{-4}
8.5	0.16837	1.39193	0.00031	0.11276	5.80×10^{-4}
9	0.15	1.32661	0.00026	0.12319	6.75×10^{-4}
9.5	0.14887	1.26948	0.00021	0.13742	7.35×10^{-4}
10	0.10892	1.2154	0.00017	0.17375	8.23×10^{-4}
10.5	0.048	1.16318	0.00011	0.22625	9.45×10^{-4}
11	0.02083	1.11939	0.00008	0.26261	9.66×10^{-4}
11.5	0.02616	1.07798	0.00006	0.28468	8.94×10^{-4}
12	0.00596	1.03529	0.00004	0.29346	6.42×10^{-4}

Table S18. Best fitted parameters (χ_T, χ_S, τ and α) with the extended Debye model for compound **6** under 0 Oe in the temperature range 2–12K.

T/ K	χ_S / cm^3 mol^{-1}	χ_T / cm^3 mol^{-1}	τ_1/s	α_1	τ_2/s	α_2	β	R
2	0.58538	5.69998	0.00247	0.23	0.1516	0.08993	0.6643	1.14×10^{-4}
2.5	0.50647	5.2	0.00248	0.23	0.15836	0.11845	0.68724	6.69×10^{-5}
3	0.44751	4.79894	0.00244	0.23	0.17083	0.15143	0.69109	4.47×10^{-5}
3.5	0.40105	4.39311	0.00233	0.22997	0.16046	0.14664	0.70321	3.49×10^{-5}
4	0.38159	3.96999	0.00208	0.21108	0.1191	0.13274	0.7099	3.61×10^{-5}
4.5	0.37616	3.56528	0.0017	0.17607	0.07446	0.11571	0.70998	2.95×10^{-5}
5	0.36301	3.2314	0.00131	0.14276	0.04603	0.10099	0.70998	2.37×10^{-5}
5.5	0.32486	2.99477	0.0098	0.13	0.02946	0.10569	0.70995	3.23×10^{-5}
6	0.28061	2.81198	0.0071	0.13	0.01933	0.11814	0.71	7.23×10^{-5}
6.5	0.23757	2.64668	0.0051	0.13	0.0125	0.12927	0.71	1.27×10^{-4}
7	0.20605	2.50029	0.0037	0.13001	0.0084	0.13311	0.70999	1.53×10^{-4}
7.5	0.20009	2.34313	0.0028	0.13002	0.00559	0.13152	0.70999	1.67×10^{-4}
8	0.20012	2.20066	0.0021	0.13	0.0037	0.13051	0.70998	1.52×10^{-4}
8.5	0.17064	2.10992	0.0015	0.1421	0.00184	0.21136	0.66387	1.84×10^{-4}
9	0.20253	1.9516	0.0012	0.13068	0.00144	0.11051	0.70998	6.12×10^{-5}
9.5	0.29949	1.75269	0.0078	0.13002	0.00001	0.06023	0.37098	4.11×10^{-5}
10	0.29596	1.67162	0.0022	0.16587	0.00004	0.37386	0.70971	8.18×10^{-5}
10.5	0.08802	1.78703	0.0016	0.1304	0	0.41523	0.70534	4.33×10^{-5}
11	0.19063	1.61378	0.0011	0.13106	0	0.43864	0.70298	5.66×10^{-5}
11.5	0.17385	1.55152	0.0012	0.13471	0.00003	0.06591	0.31232	4.76×10^{-5}
12	0.14456	1.8073	0.00004	0.13005	0	0.41462	0.70971	3.10×10^{-5}

Table S19. The curves are fitted by QTM, Raman and Orbach process for complexes **1**-**6**.

complex	dc field		q(s^{-1})	C ($s^{-1}\cdot K^{-n}$)	n	τ_0 (s)	$U_{eff}/\kappa B$ (K)
complex **1**	zero dc field	Value	0.0057	22.2045	1.002	1.442×10^{-5}	28.34
		Standard Error	2.45×10^{-5}	4.19×10^{-1}	1.2×10^{-1}	2.47×10^{-8}	1.21
complex **2**	zero dc field	Value	0.0159	0.01865	4.0165	4.68×10^{-5}	27.61
		Standard Error	1.21×10^{-4}	3.41×10^{-4}	2.3×10^{-1}	3.46×10^{-8}	2.38
complex **3**	zero dc field	Value	0.0027	0.03897	5.8087	9.52×10^{-5}	34.21
		Standard Error	6.54×10^{-5}	5.46×10^{-4}	5.7×10^{-1}	6.48×10^{-7}	2.98
complex **4**	zero dc field	Value	0.0135	0.47243	3.6113	9.31×10^{-6}	61.23
		Standard Error	5.16×10^{-5}	2.86×10^{-3}	4.66×10^{-1}	5.73×10^{-8}	1.65
complex **5**	zero dc field	Value	0.0026	19.3645	1.8624	6.83×10^{-5}	34.54
		Standard Error	1.91×10^{-4}	8.37×10^{-2}	3.81×10^{-1}	2.39×10^{-7}	1.49
complex **6**	zero dc field	Value	0.0006	10.8342	0.9926	9.63×10^{-5}	36.03
		Standard Error	2.79×10^{-5}	6.53×10^{-2}	8.63×10^{-2}	5.52×10^{-7}	2.04

Table S20. The curves are fitted by Raman and Orbach process for complexes **1**-**6** under applied dc field.

complex	dc field		C ($s^{-1}\cdot K^{-n}$)	n	τ_0 (s)	U_{eff}/κ_B (K)
complex **1**	900 Oe dc field	Value	19.8541	1.1201	1.58×10^{-5}	28.47
		Standard Error	5.61×10^{-1}	5.31×10^{-2}	2.68×10^{-7}	1.01
complex **2**	2100 Oe dc field	Value	0.01794	4.0212	1.87×10^{-6}	26.81
		Standard Error	3.27×10^{-4}	2.16×10^{-1}	4.35×10^{-8}	2.47
complex **3**	800 Oe dc field	Value	0.03464	5.7421	3.58×10^{-6}	34.74
		Standard Error	4.97×10^{-4}	3.28×10^{-1}	5.36×10^{-8}	3.35
complex **4**	1500 Oe dc field	Value	0.50321	3.7465	3.53×10^{-6}	59.63
		Standard Error	2.08×10^{-3}	5.76×10^{-1}	6.12×10^{-8}	1.55

complex **5**	1500 Oe dc field	Value	21.7173	1.8456	9.78×10^{-6}	35.25
		Standard Error	5.37×10^{-2}	2.34×10^{-1}	4.92×10^{-7}	2.07
complex **6**	1500 Oe dc field	Value	10.8855	1.0301	6.22×10^{-6}	36.40
		Standard Error	7.36×10^{-2}	2.46×10^{-2}	3.57×10^{-8}	3.24

Table S21. The curves are fitted by Raman and Orbach process for complexes **7** and **8** under applied dc field.

complex	dc field		C ($s^{-1}\cdot K^{-n}$)	n	τ_0 (s)	U_{eff}/κ_B (K)
complex **7**	1100 Oe dc field	Value	34.9133	1.5782	1.65×10^{-6}	26.06
		Standard Error	5.25×10^{-1}	1.67×10^{-1}	3.24×10^{-8}	1.06
complex **8**	1100 Oe dc field	Value	32.8521	1.8309	7.16×10^{-8}	40.77
		Standard Error	4.83×10^{-1}	2.93×10^{-1}	1.33×10^{-9}	2.34

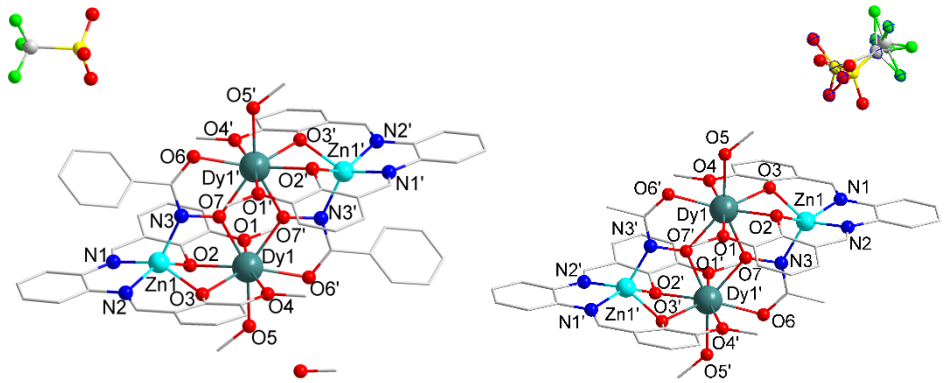

Fig. S1 Partially labeled molecular structure of complexes **2** (left) and **3** (right). The minor part of the disorder $CF_3SO_3^{-1}$ is shown as front ellipse in blue line. Color code: Dy (teal), Zn (light blue), O (red), N (blue), C (grey), S (yellow), F (green).

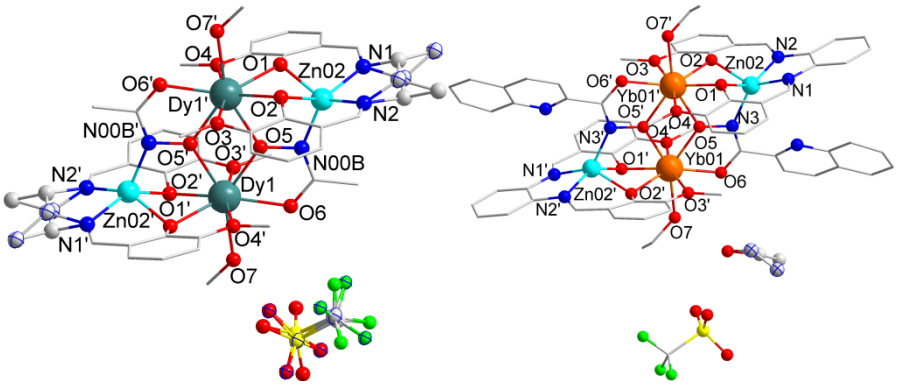

Fig. S2 Partially labeled molecular structure of complexes **5** (left) and **7** (right). The minor part of the disorder $CF_3SO_3^{-1}$ is shown as front ellipse in blue line. Color code: Dy (teal), Zn (light blue), O (red), N (blue), C (grey), S (yellow), F (green).

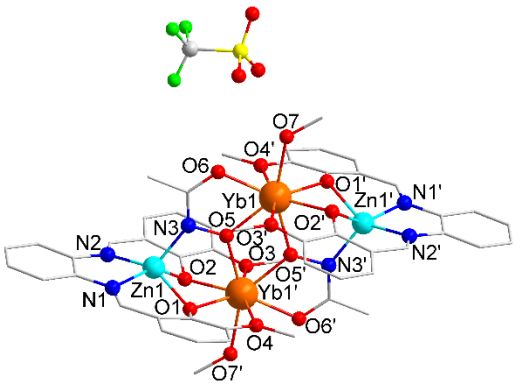

Fig. S3 Partially labeled molecular structure of complexes **8**. Color code: Dy (teal), Yb (orange), Zn (light blue), O (red), N (blue), C (grey), S (yellow), F (green).

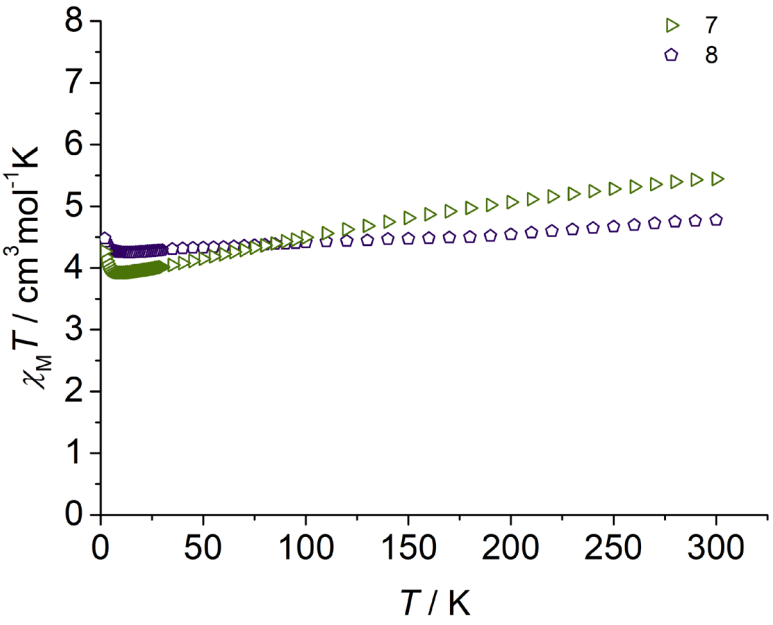

Fig. S4 Temperature dependence of the magnetic susceptibility $\chi_M T$ at 1000 Oe for complexes **7** and **8**.

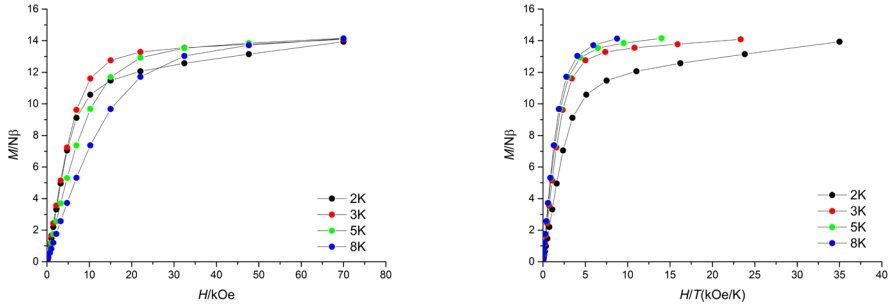

Fig. S5 Field dependences of magnetization in the field range 0–70 kOe and temperature range 2–8 K for **1**.

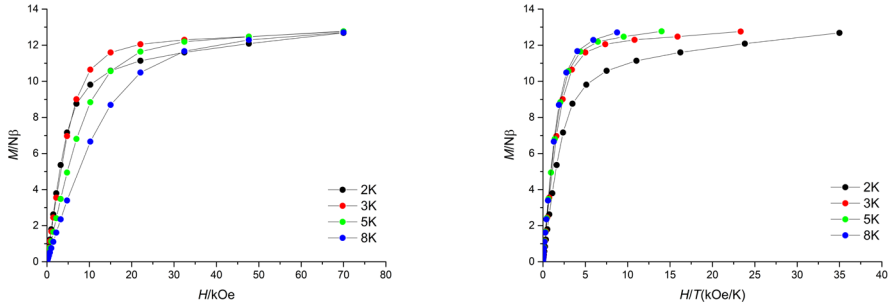

Fig. S6 Field dependences of magnetization in the field range 0–70 kOe and temperature range 2–8 K for **2**.

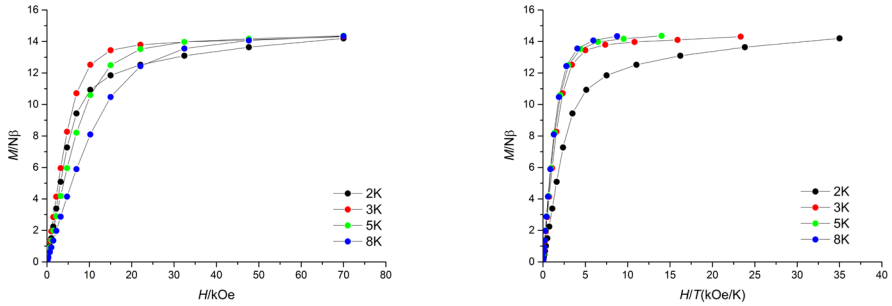

Fig. S7 Field dependences of magnetization in the field range 0–70 kOe and temperature range 2–8 K for **3**.

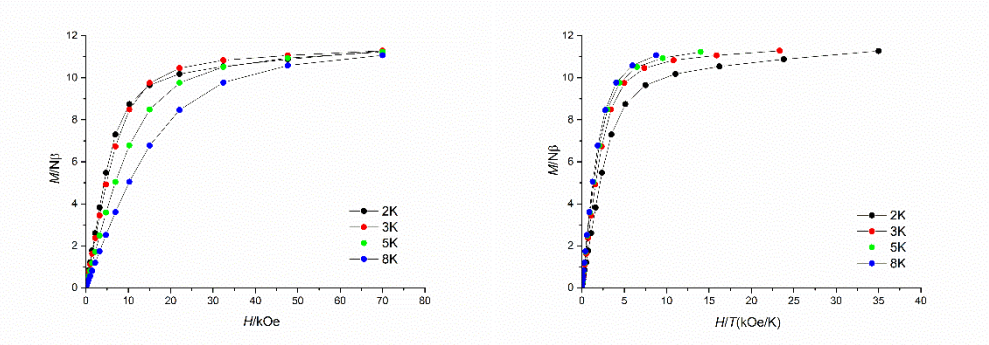

Fig. S8 Field dependences of magnetization in the field range 0–70 kOe and temperature range 2–8 K for **4**.

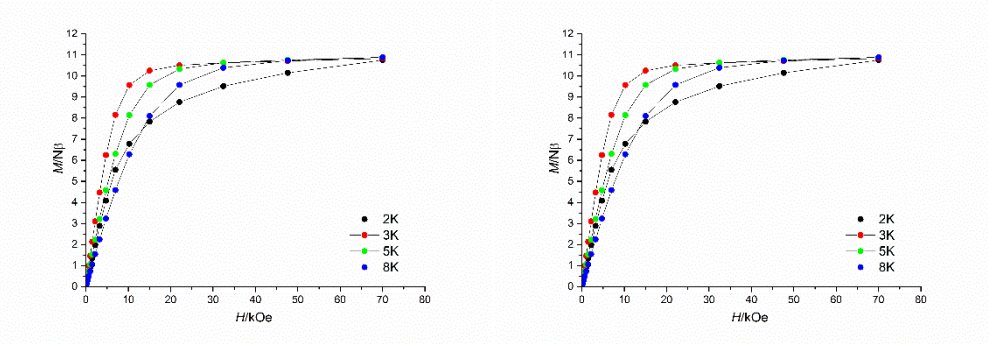

Fig. S9 Field dependences of magnetization in the field range 0–70 kOe and temperature range 2–8 K for **5**.

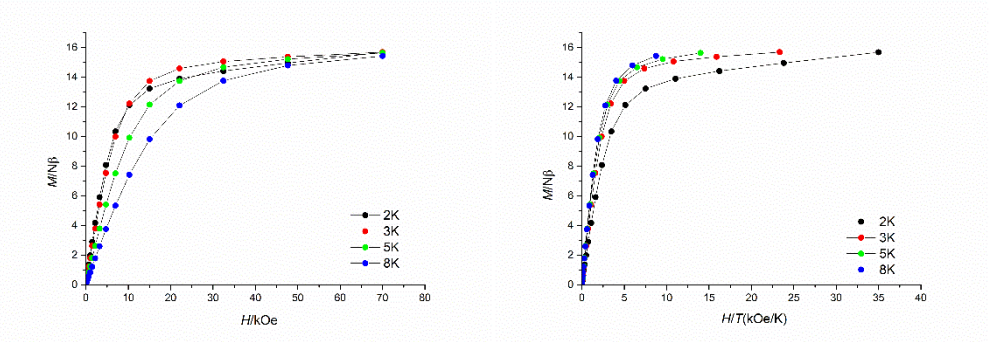

Fig. S10 Field dependences of magnetization in the field range 0–70 kOe and temperature range 2–8 K for **6**.

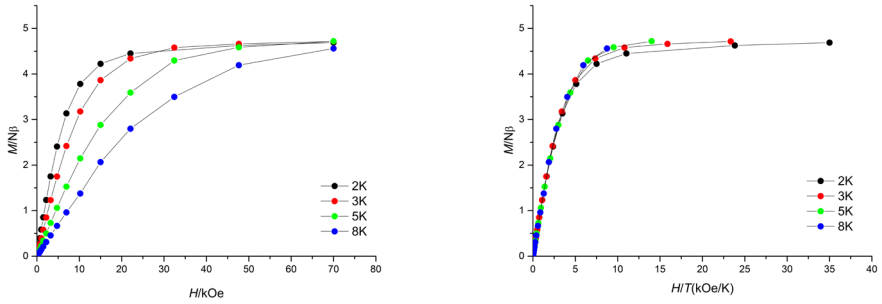

Fig. S11 Field dependences of magnetization in the field range 0–70 kOe and temperature range 2–8 K for **7**.

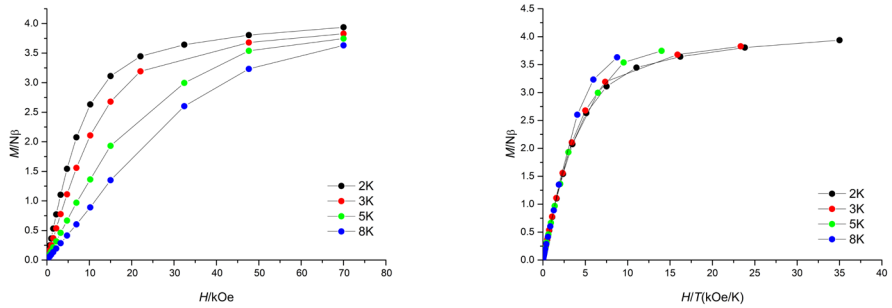

Fig. S12 Field dependences of magnetization in the field range 0–70 kOe and temperature range 2–8 K for **8**.

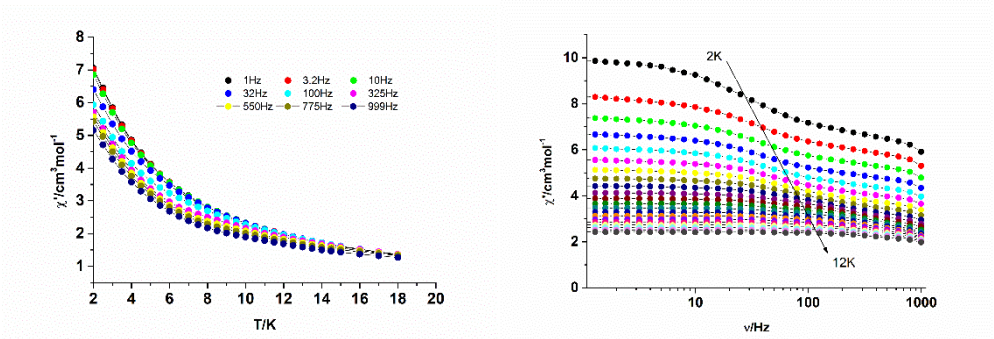

Fig. S13 The temperature and frequency dependence of the in-phase (χ') ac susceptibility component under zero field for complex **1**.

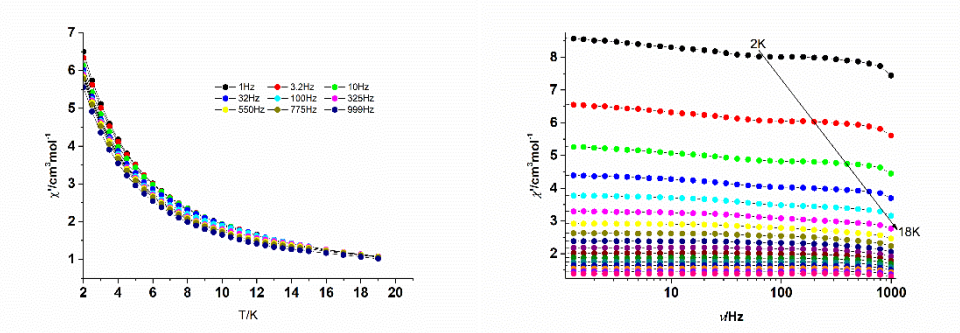

Fig. S14 The temperature and frequency dependence of the in-phase (χ') ac susceptibility component under zero field for complex **2**.

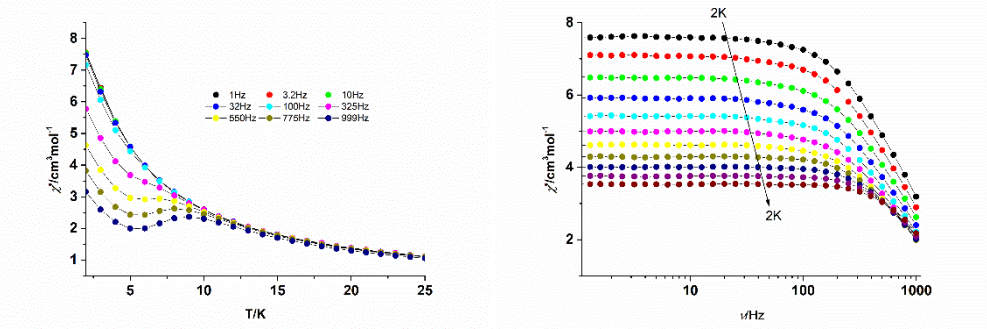

Fig. S15 The temperature and frequency dependence of the in-phase (χ') ac susceptibility component under zero field for complex **3**.

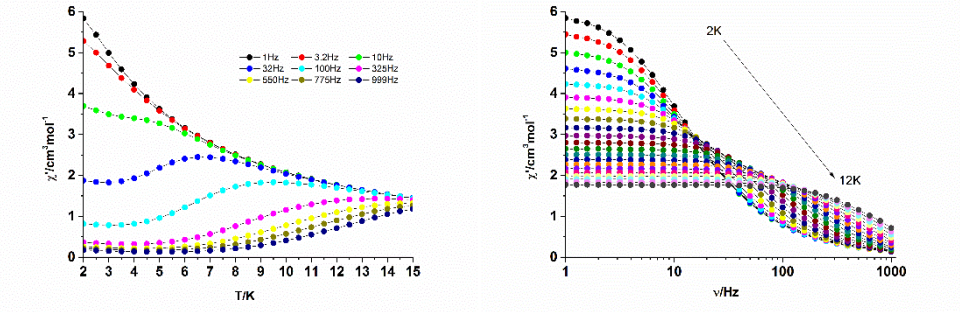

Fig. S16 The temperature and frequency dependence of the in-phase (χ') ac susceptibility component under zero field for complex **4**.

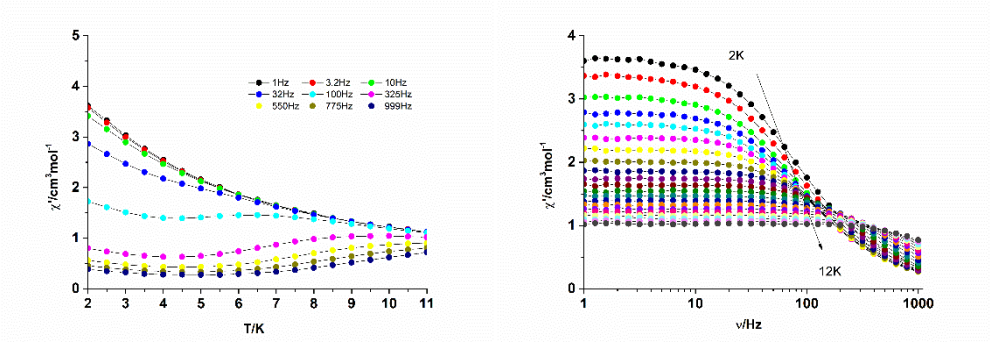

Fig. S17 The temperature and frequency dependence of the in-phase (χ') ac susceptibility component under zero field for complex **5**.

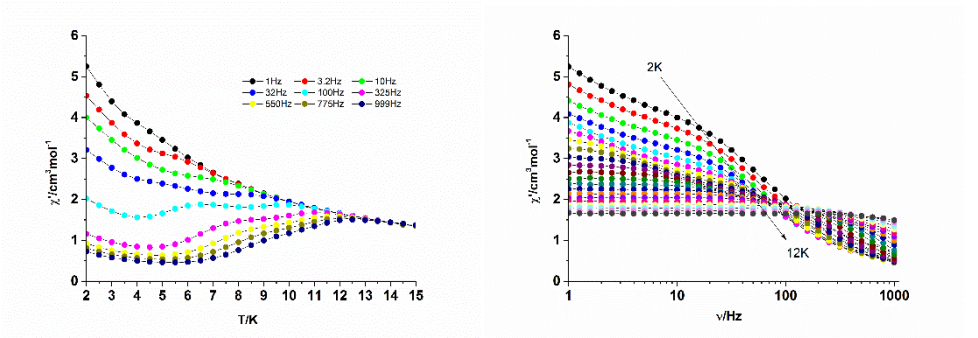

Fig. S18 The temperature and frequency dependence of the in-phase (χ') ac susceptibility component under zero field for complex **6**.

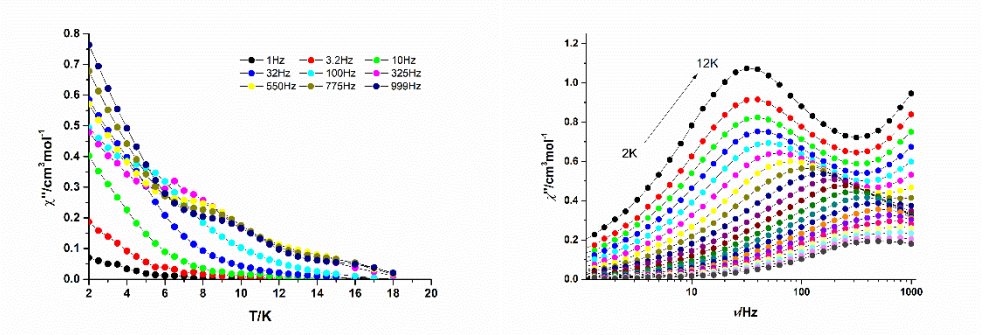

Fig. S19 The temperature and frequency dependence of the in-phase (χ'') ac susceptibility component under zero field for complex **1**.

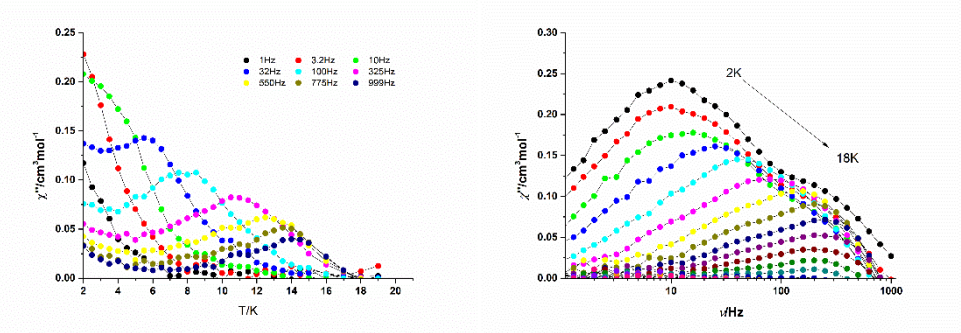

Fig. S20 The temperature and frequency dependence of the in-phase (χ'') ac susceptibility component under zero field for complex **2**.

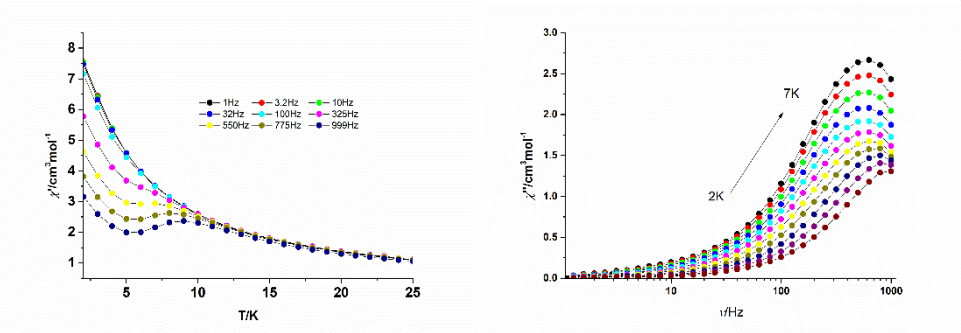

Fig. S21 The temperature and frequency dependence of the in-phase (χ'') ac susceptibility component under zero field for complex **3**.

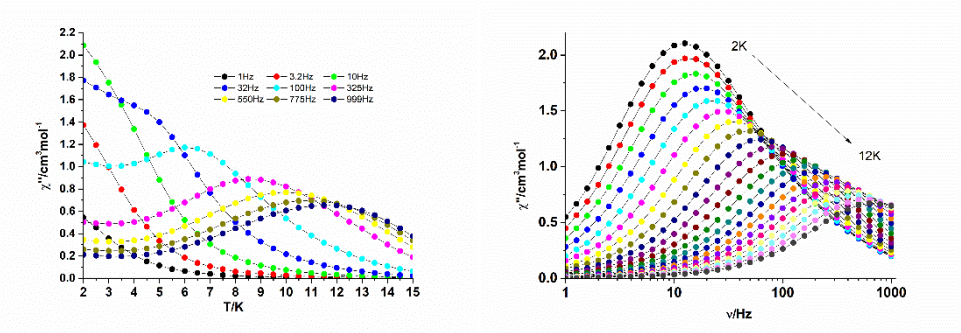

Fig. S22 The temperature and frequency dependence of the in-phase (χ'') ac susceptibility component under zero field for complex **4**.

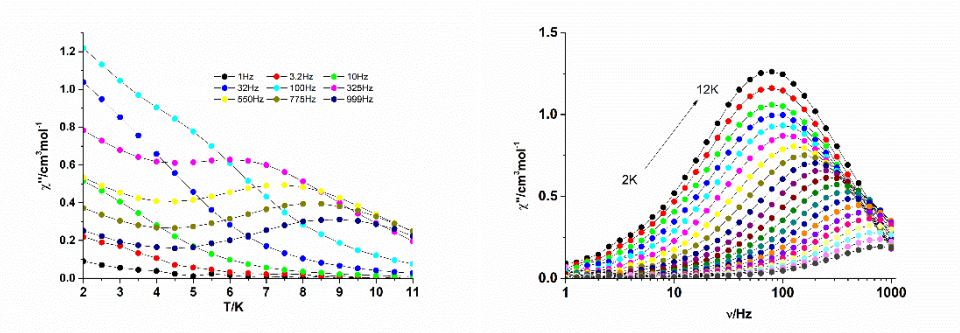

Fig. S23 The temperature and frequency dependence of the in-phase (χ'') ac susceptibility component under zero field for complex **5**.

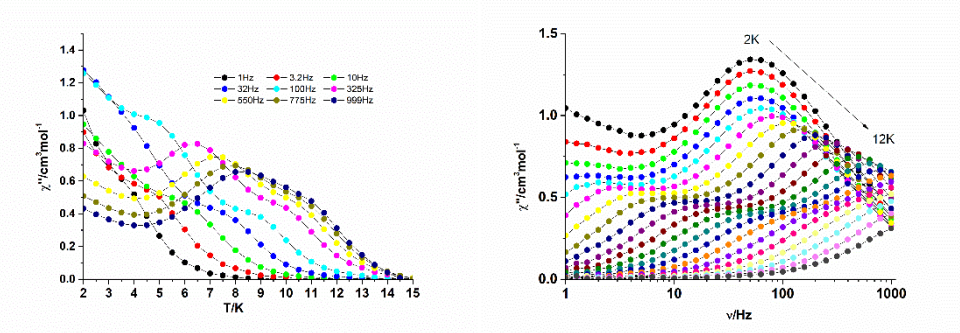

Fig. S24 The temperature and frequency dependence of the in-phase (χ'') ac susceptibility component under zero field for complex **6.**

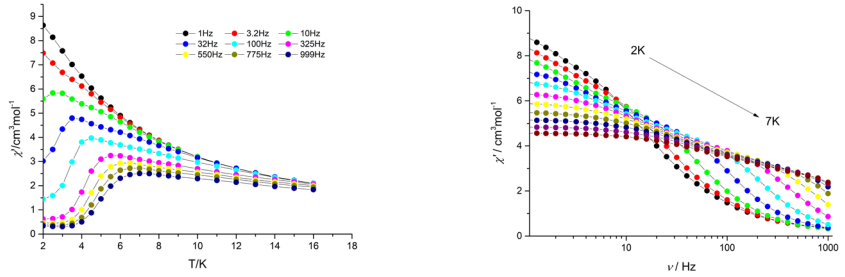

Fig. S25 The temperature and frequency dependence of the in-phase (χ') ac susceptibility component under 900 Oe for complex **1**.

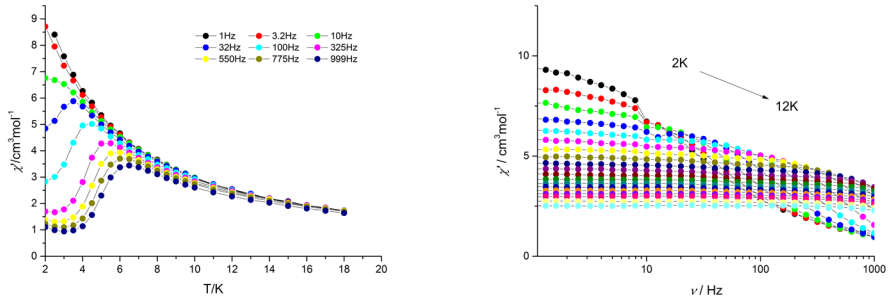

Fig. S26 The temperature and frequency dependence of the in-phase (χ') ac susceptibility component under 2100 Oe for complex **2**.

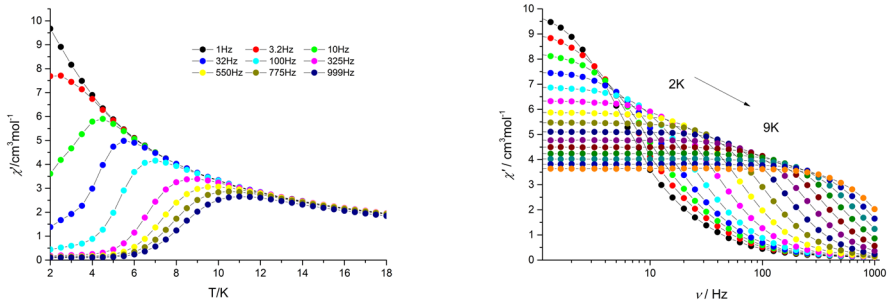

Fig. S27 The temperature and frequency dependence of the in-phase (χ') ac susceptibility component under 800 Oe for complex **3**.

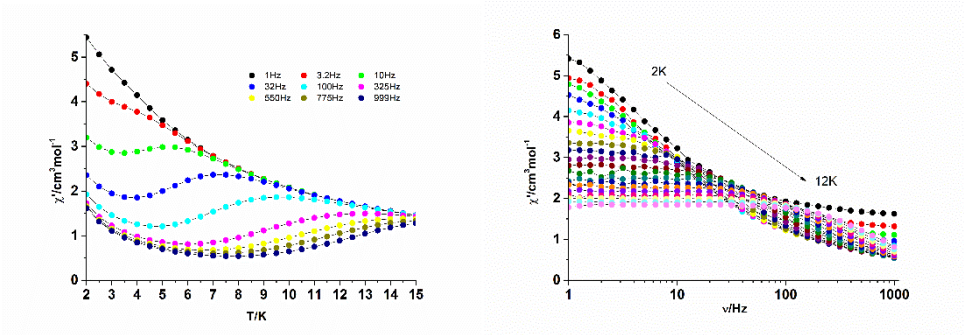

Fig. S28 The temperature and frequency dependence of the in-phase (χ') ac susceptibility component under 1500 Oe for complex **4**.

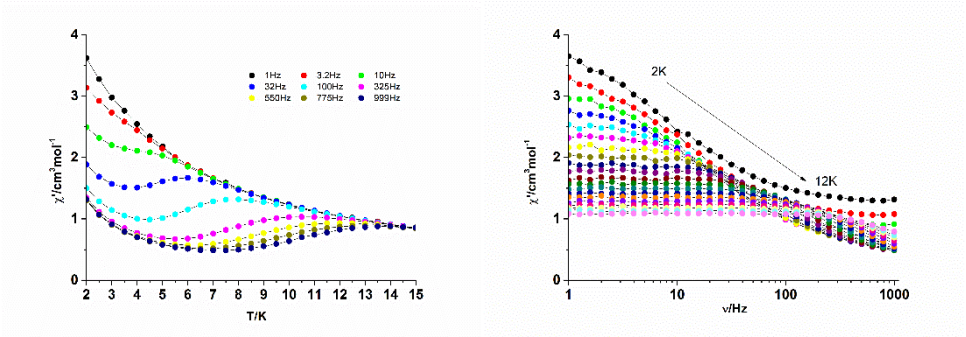

Fig. S29 The temperature and frequency dependence of the in-phase (χ') ac susceptibility component under 1500 Oe for complex **5**.

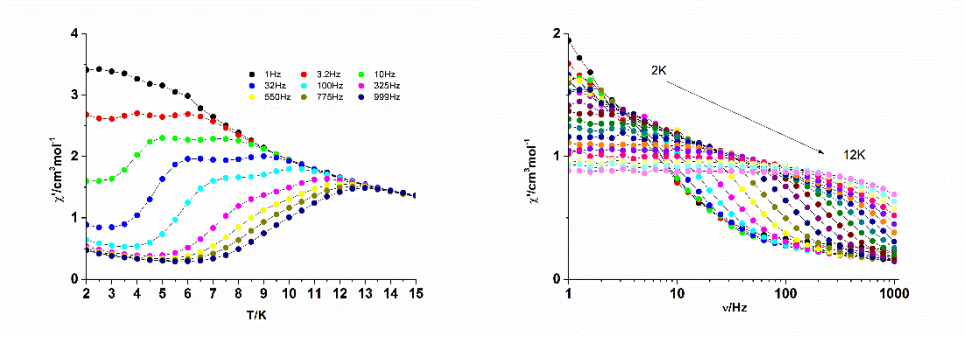

Fig. S30 The temperature and frequency dependence of the in-phase (χ') ac susceptibility component under 1500 Oe for complex **6**.

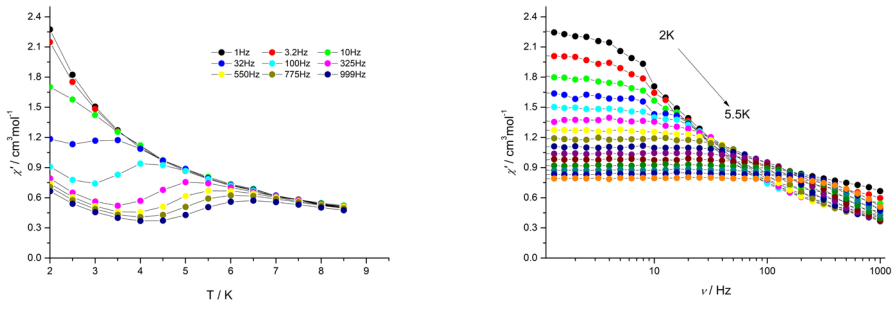

Fig. S31 The temperature and frequency dependence of the in-phase (χ') ac susceptibility component under 1100 Oe for complex **7**.

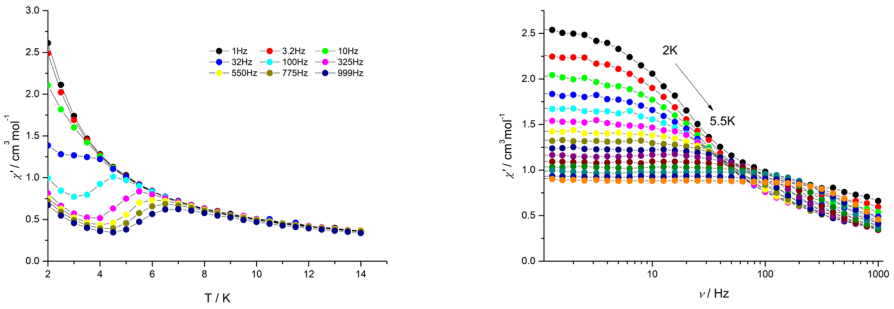

Fig. S32 The temperature and frequency dependence of the in-phase (χ') ac susceptibility component under 1100 Oe for complex **8**.

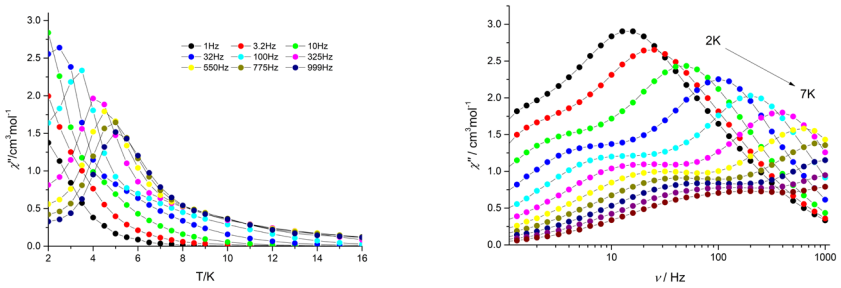

Fig. S33 The temperature and frequency dependence of the in-phase (χ'') ac susceptibility component under 900 Oe for complex **1**.

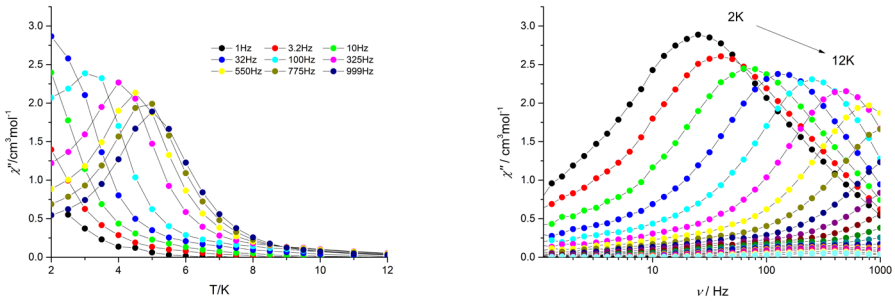

Fig. S34 The temperature and frequency dependence of the in-phase (χ'') ac susceptibility component under 2100 Oe for complex **2**.

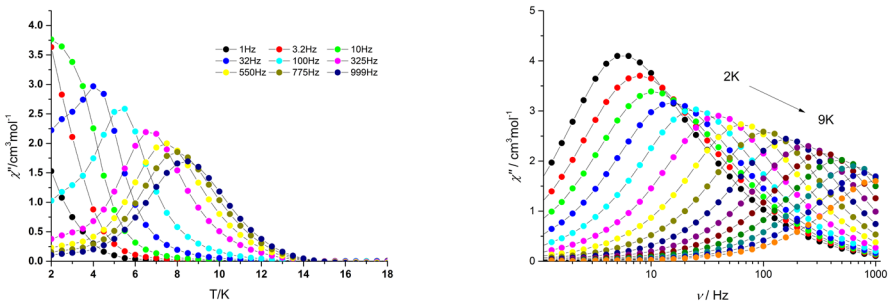

Fig. S35 The temperature and frequency dependence of the in-phase (χ'') ac susceptibility component under 900 Oe for complex **3**.

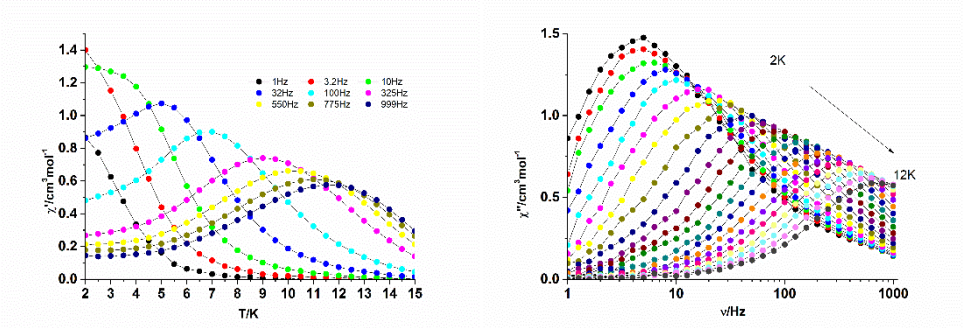

Fig. S36 The temperature and frequency dependence of the in-phase (χ'') ac susceptibility component under 1500 Oe for complex **4**.

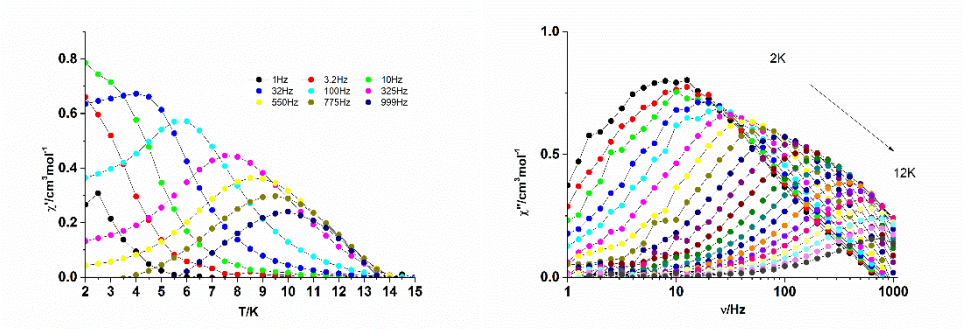

Fig. S37 The temperature and frequency dependence of the in-phase (χ'') ac susceptibility component under 1500 Oe for complex **5**.

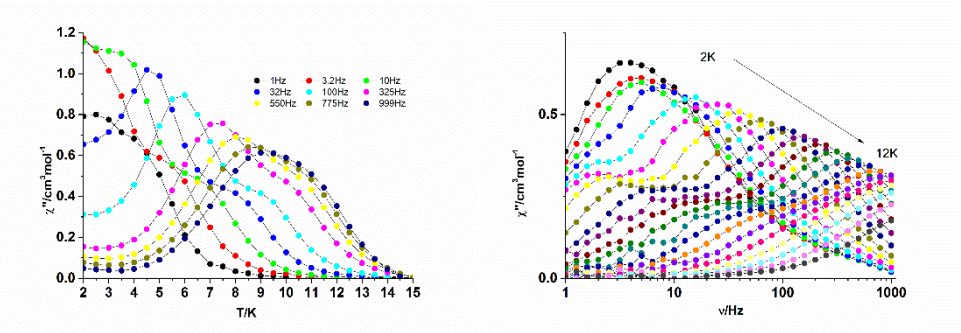

Fig. S38 The temperature and frequency dependence of the in-phase (χ'') ac susceptibility component under 1500 Oe for complex **6**.

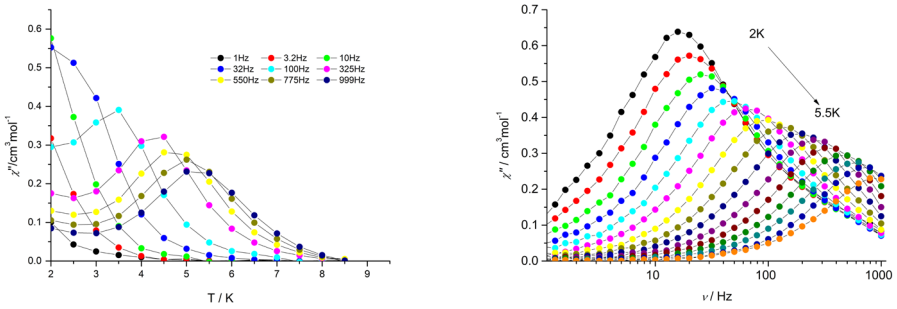

Fig. S39 The temperature and frequency dependence of the in-phase (χ'') ac susceptibility component under 1100 Oe for complex **7**.

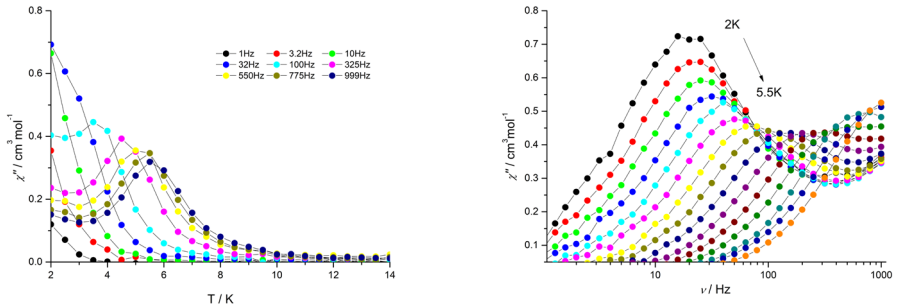

Fig. S40 The temperature and frequency dependence of the in-phase (χ'') ac susceptibility component under 1100 Oe for complex **8**.

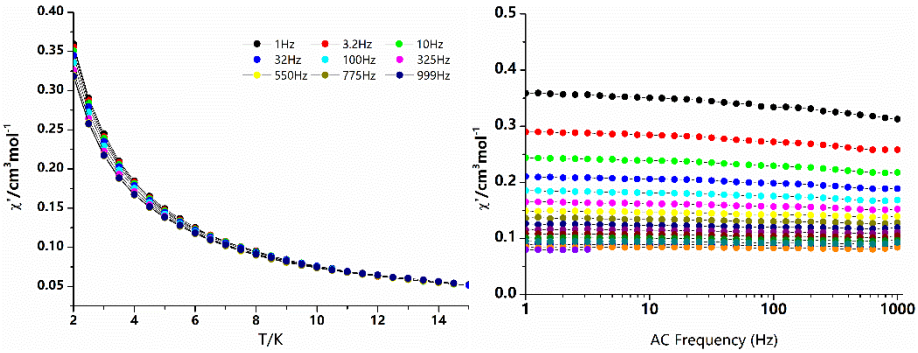

Fig. S41 The temperature and frequency dependence of the in-phase (χ') ac susceptibility component under zero field for complex **2a**.

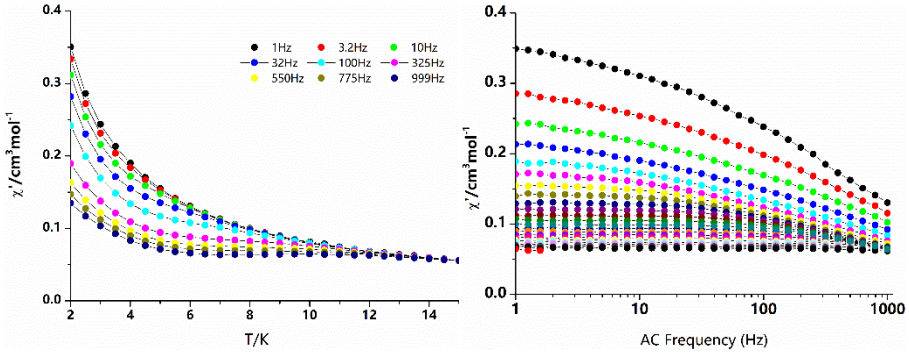

Fig. S42 The temperature and frequency dependence of the in-phase (χ') ac susceptibility component under zero field for complex **6a**.

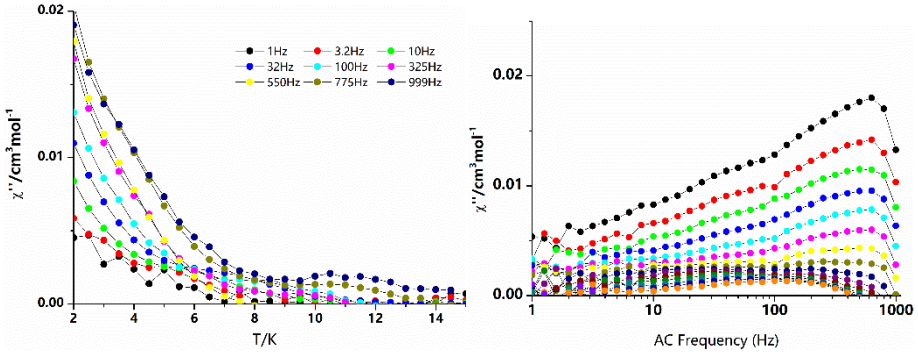

Fig. S43 The temperature and frequency dependence of the in-phase (χ'') ac susceptibility component under zero field for complex **2a**.

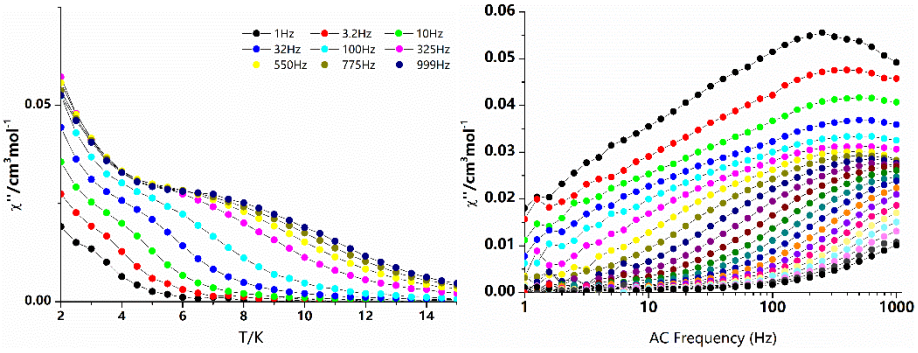

Fig. S44 The temperature and frequency dependence of the in-phase (χ'') ac susceptibility component under zero field for complex **6a**.

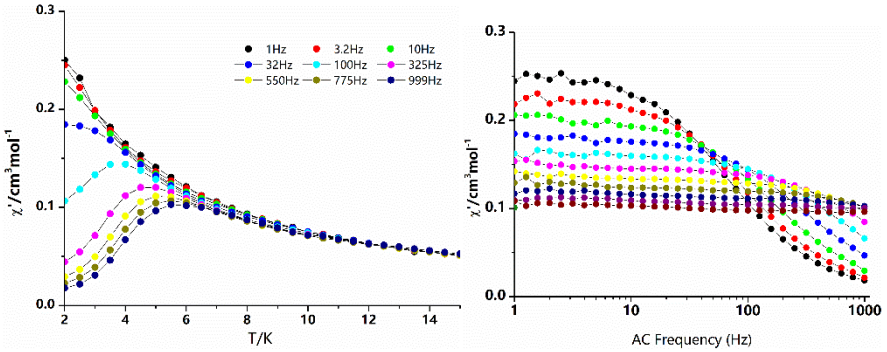

Fig. S45 The temperature and frequency dependence of the in-phase (χ') ac susceptibility component under 2100 Oe for complex **2a**.

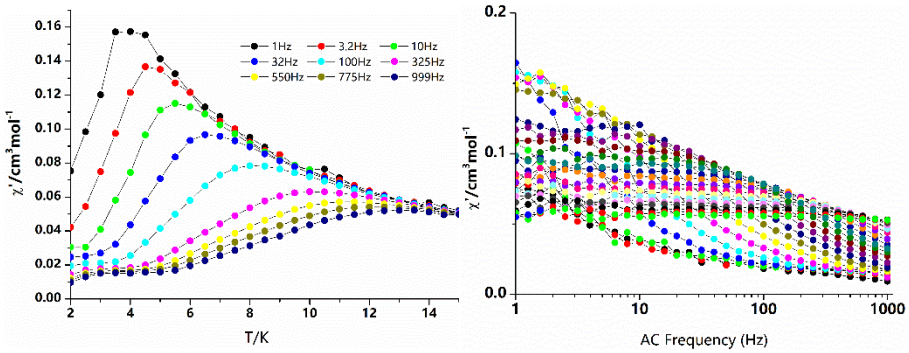

Fig. S46 The temperature and frequency dependence of the in-phase (χ') ac susceptibility component under 1500 Oe for complex **6a**.

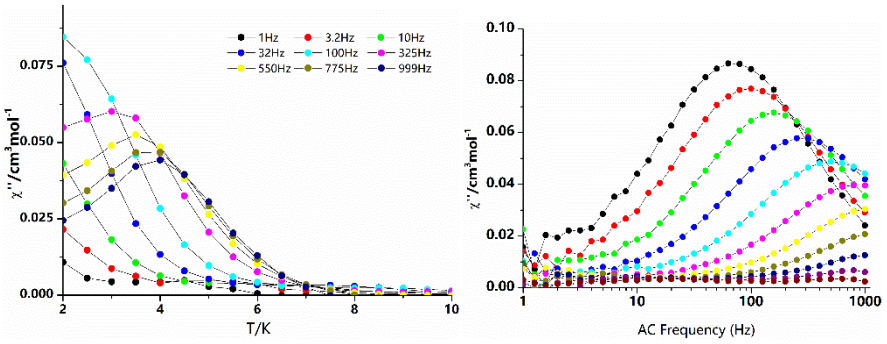

Fig. S47 The temperature and frequency dependence of the in-phase (χ'') ac susceptibility component under 2100 Oe for complex **2a**.

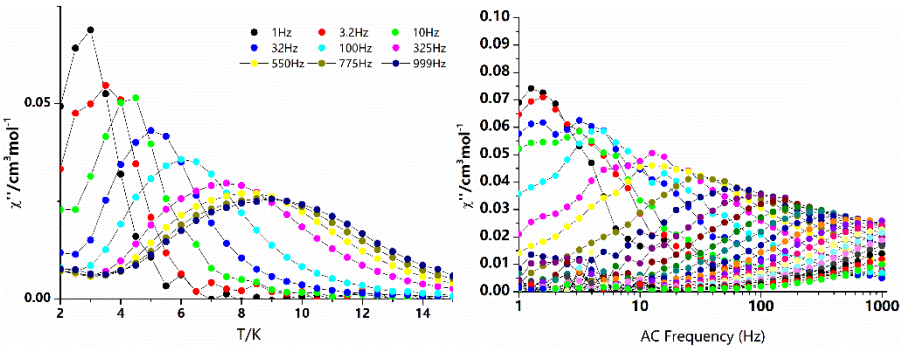

Fig. S48 The temperature and frequency dependence of the in-phase (χ'') ac susceptibility component under 1500 Oe for complex **6a**.

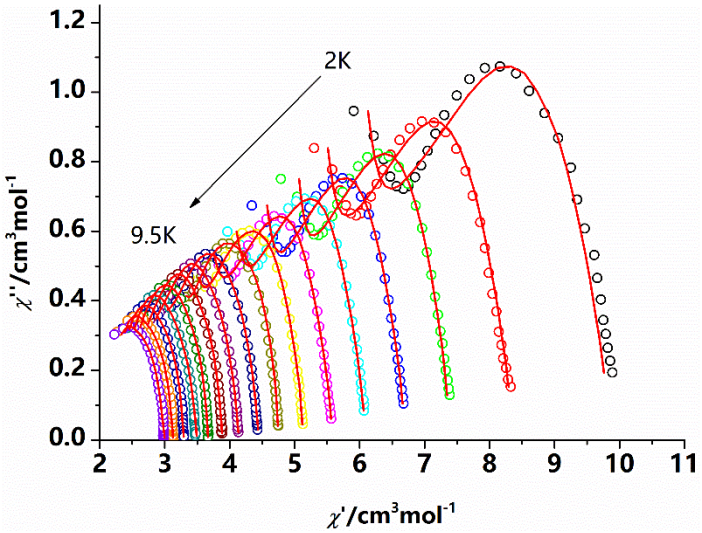

Fig. S49 Cole-Cole (Argand) plot for **1** obtained using the ac susceptibility data. The solid lines correspond to the best fit obtained with a generalized Debye model under zero dc field.

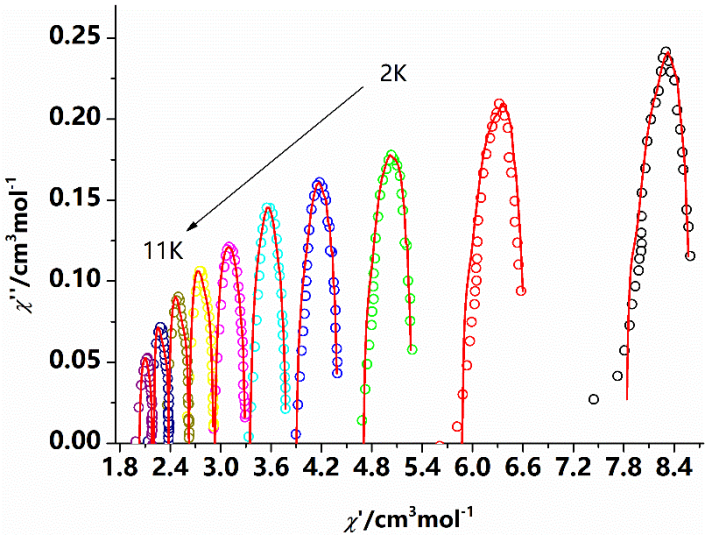

Fig. S50 Cole-Cole (Argand) plot for **2** obtained using the ac susceptibility data. The solid lines correspond to the best fit obtained with a generalized Debye model under zero dc field.

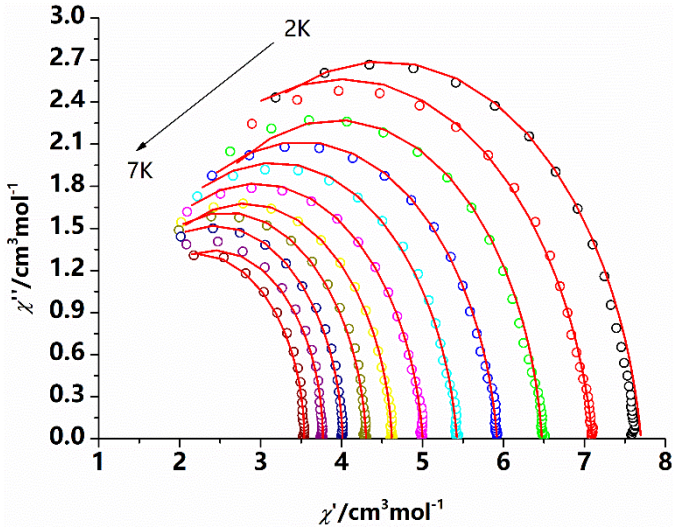

Fig. S51 Cole-Cole (Argand) plot for **3** obtained using the ac susceptibility data. The solid lines correspond to the best fit obtained with a generalized Debye model under zero dc field.

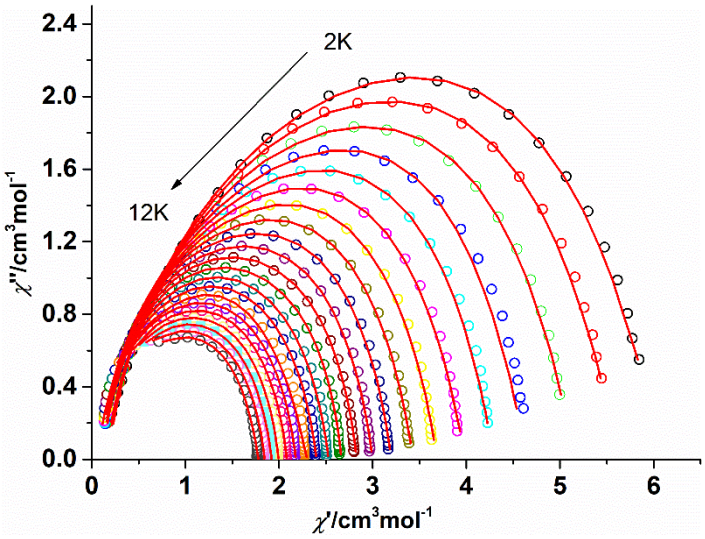

Fig. S52 Cole-Cole (Argand) plot for **4** obtained using the ac susceptibility data. The solid lines correspond to the best fit obtained with a generalized Debye model under zero dc field.

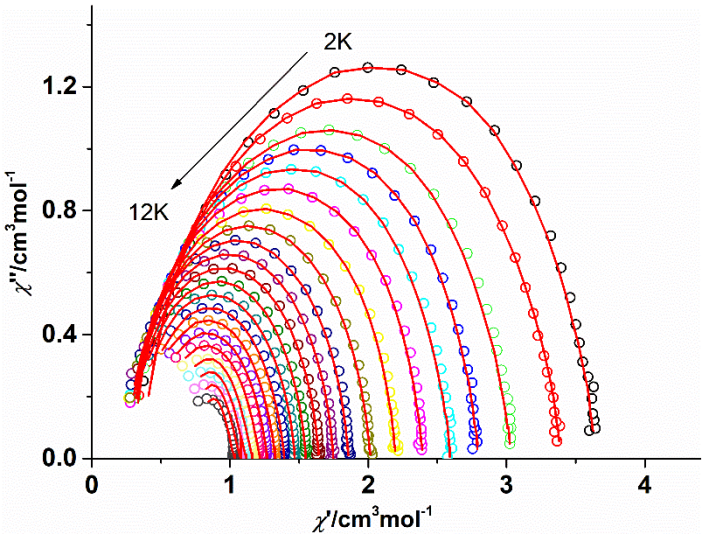

Fig. S53 Cole-Cole (Argand) plot for **5** obtained using the ac susceptibility data. The solid lines correspond to the best fit obtained with a generalized Debye model under zero dc field.

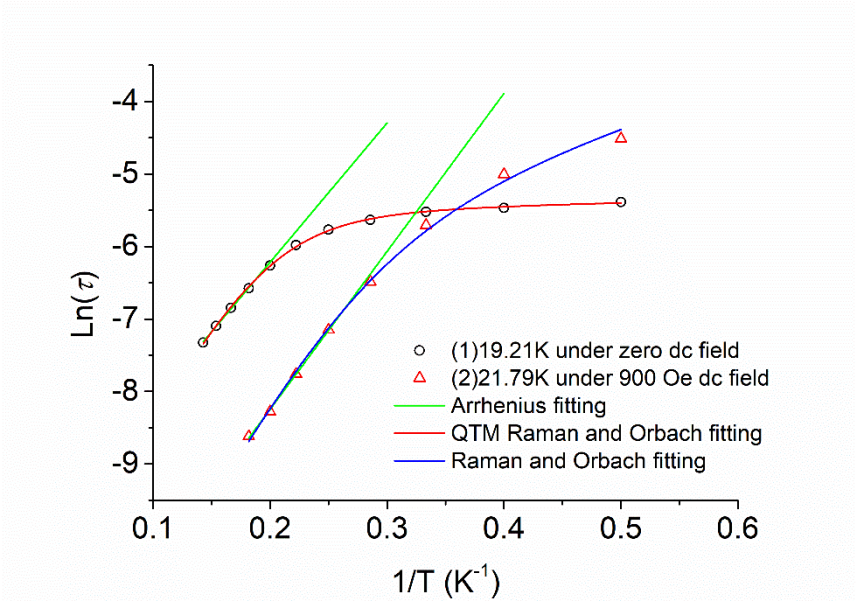

Fig. S54 Plots of ln(τ) versus 1/T at zero dc field and out of dc field for **1**. The red solid lines represent the fitting of the frequency data by Equation 1, blue dotted lines by Equation 2, and the green solid lines represent the pure Arrhenius fitting, respectively.

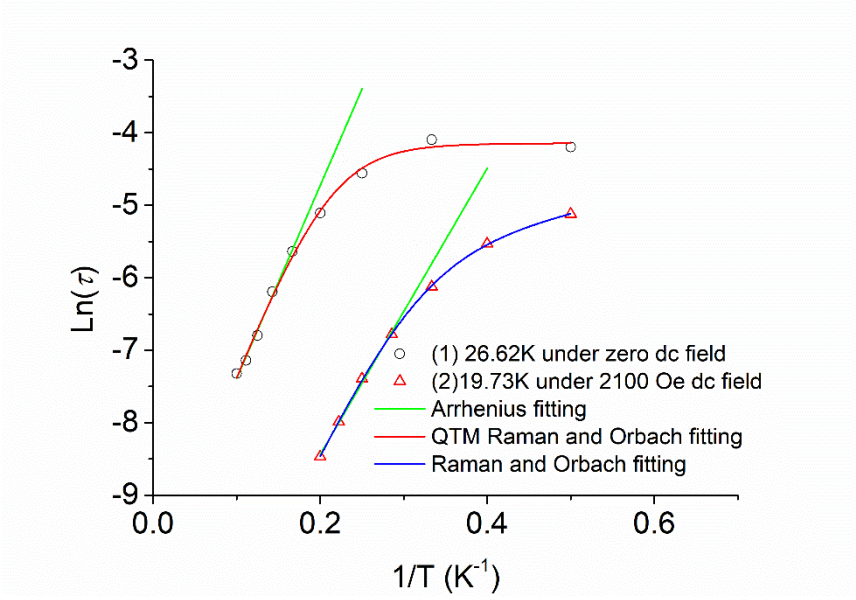

Fig. S55 Plots of ln(τ) versus 1/T at zero dc field and out of dc field for **2**. The red solid lines represent the fitting of the frequency data by Equation 1, blue dotted lines by Equation 2, and the green solid lines represent the pure Arrhenius fitting, respectively.

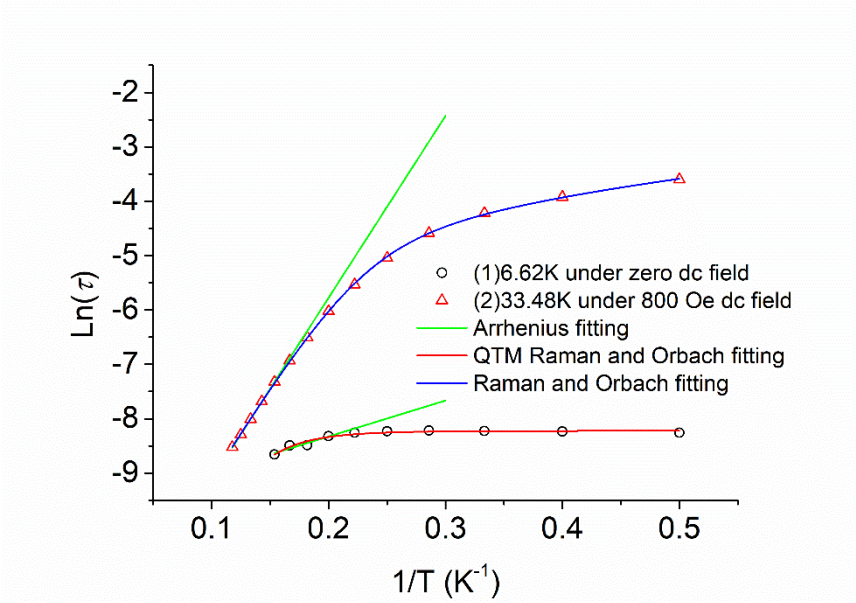

Fig. S56 Plots of ln(τ) versus 1/T at zero dc field and out of dc field for **3**. The red solid lines represent the fitting of the frequency data by Equation 1, blue dotted lines by Equation 2, and the green solid lines represent the pure Arrhenius fitting, respectively.

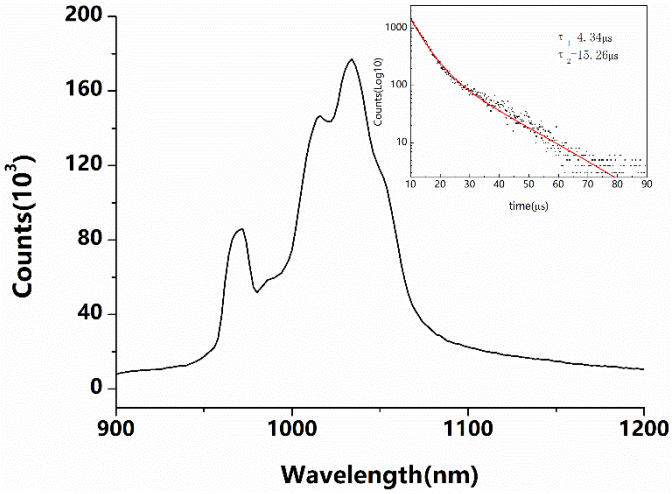

Fig. S57 Emission spectrum at λex = 310 nm at 77 K and Luminescence decay profiles of complex **7**.

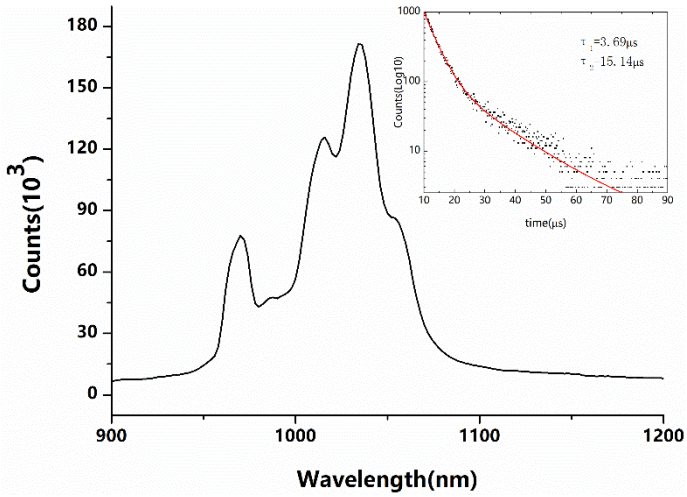

Fig. S58 Emission spectrum at λex = 310 nm at 77 K and Luminescence decay profiles of complex **8.**

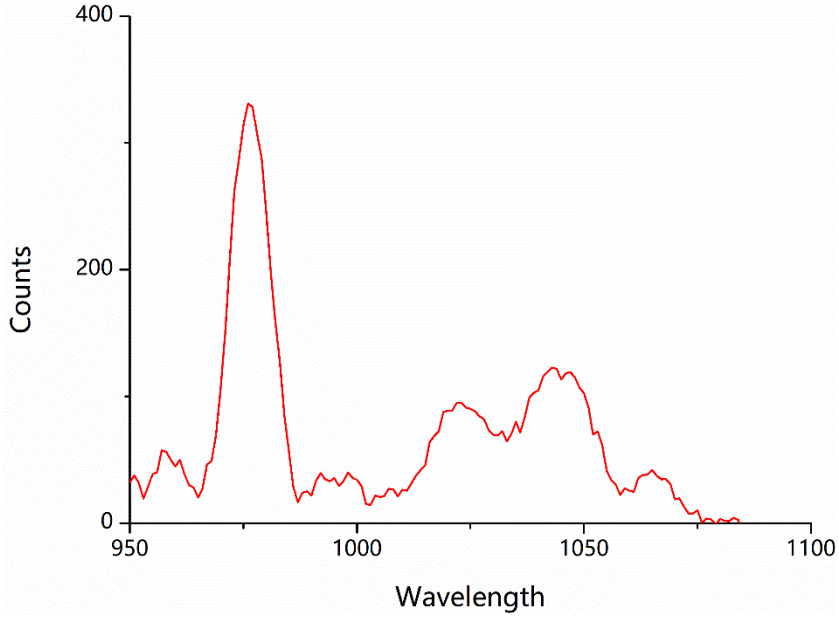

Fig. S59 Emission spectrum at λex = 310 nm at 75 K and Luminescence decay profiles of complex **8**.

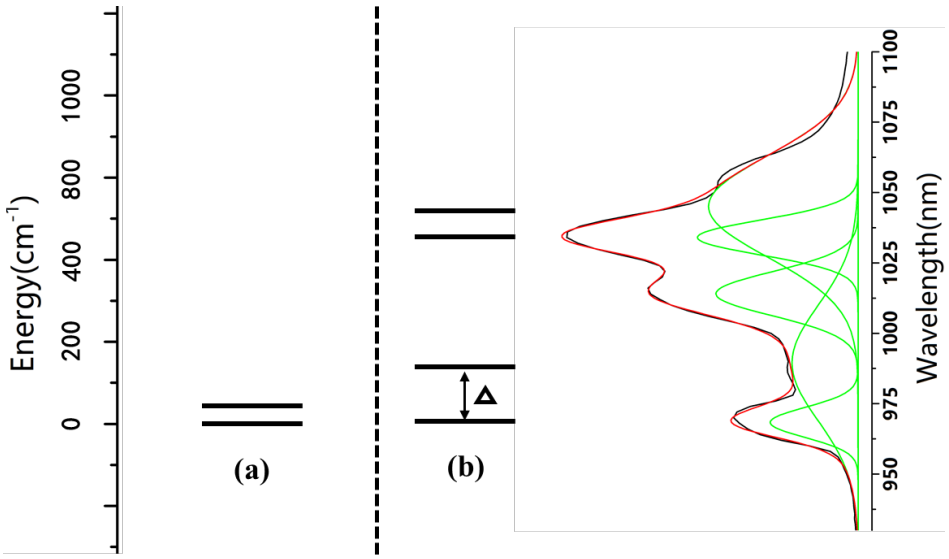

Fig. S60 Energy levels of the $^2F_{7/2}$ ground state multiple determined from (a) ac fit (U_{eff}/k_B=18.6 cm^{-1}), and (b) the luminescence spectrum of complex **7** (Δ=178cm^{-1}). The area of Gaussian deconvolution corresponding to the four Kramers doublets and one hot transition.

Computational details

Both of binuclear complexes **2** and **4** have one type of molecular structure. For binuclear complex **6**, it has two types of molecular structures indicated as **6_*a*** and **6_*b***. Each of them has one type of magnetic center Dy^{III} ion due to their centrosymmetric structures. Complete-active-space self-consistent field (CASSCF) calculations on individual Dy^{III} fragments for complexes **2, 4** and **6** (see Fig. S61 for the calculated complete structures of **2, 4** and **6**) on the basis of single-crystal X-ray determined geometries have been carried out with MOLCAS 8.4[S1] program package. Each individual Dy^{III} fragment in **2, 4** and **6** was calculated keeping the experimentally determined structure of the corresponding compound while replacing the neighboring Dy^{III} ion by diamagnetic Lu^{III}.

The basis sets for all atoms are atomic natural orbitals from the MOLCAS ANO-RCC library: ANO-RCC-VTZP for Dy^{III}; VTZ for close O; VDZ for distant atoms. The calculations employed the second order Douglas-Kroll-Hess Hamiltonian, where scalar relativistic contractions were taken into account in the basis set and the spin-orbit couplings were handled separately in the restricted active space state interaction (RASSI-SO) procedure. Active electrons in 7 active orbitals include all *f* electrons (CAS (9 in 7) in the CASSCF calculation. To exclude all the doubts, we calculated all the roots in the active space. We have mixed the maximum number of spin-free state which was possible with our hardware (all from 21 sextets, 128 from 224 quadruplets, 130 from 490 doublets for Dy^{III}. SINGLE_ANISO[S2–S4] program was used to obtain the energy levels, ***g*** tensors, magnetic axes, *et al.* based on the above CASSCF/RASSI-SO calculations.

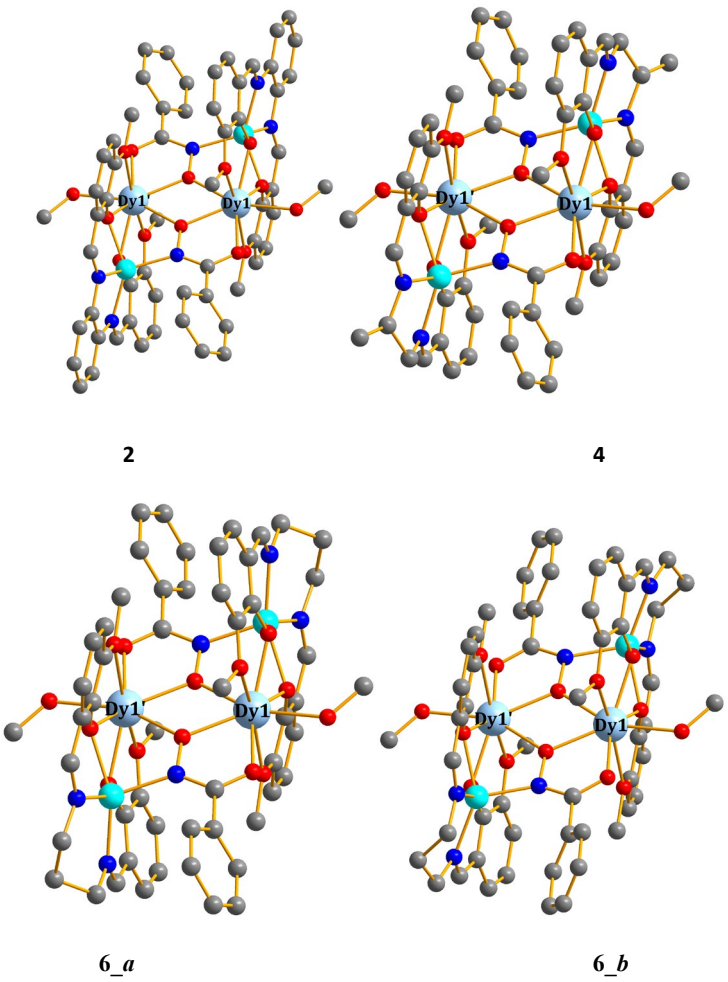

Fig. S61 Calculated complete structures of complexes **2**, **4** and **6**; H atoms are omitted for clarify.

Table S22. Calculated energy levels (cm^{-1}), g (gx, gy, gz) tensors and predominant mJ values of the lowest eight Kramers doublets (KDs) of individual DyIII fragments for complexes **2**, **4** and **6** using CASSCF/RASSI-SO with MOLCAS 8.4.

KDs	**1(Dy1)**			**2(Dy1)**			**3_*a*(Dy1)**			**3_*b*(Dy1)**		
	E/cm^{-1}	***g***	m_J	*E*/cm^{-1}	***g***	m_J	*E*/cm^{-1}	***g***	m_J	*E*/cm^{-1}	***g***	m_J
1	0.0	0.014 0.024 19.778	±15/2	0.0	0.022 0.039 19.742	±15/2	0.0	0.026 0.047 19.701	±15/2	0.0	0.025 0.046 19.681	±15/2
2	262.7	0.941 2.295 15.513	±13/2	219.5	1.050 2.463 15.915	±13/2	218.6	1.543 4.775 13.793	±13/2	197.8	0.788 1.545 16.629	±13/2
3	363.1	2.365 3.486 10.241	±11/2	311.4	1.715 3.553 10.815	±11/2	292.0	0.224 4.151 8.847	±11/2	308.3	3.101 3.513 11.401	±7/2
4	494.7	7.485 6.722 1.608	±5/2	439.6	7.739 6.725 1.772	±5/2	422.9	7.493 6.921 1.976	±5/2	422.9	7.296 6.724 1.472	±5/2
5	634.3	2.481 3.837 10.291	±3/2	570.0	2.658 3.810 10.358	±3/2	553.6	2.703 3.483 10.629	±3/2	549.5	2.715 3.144 10.839	±3/2
6	744.4	1.048 1.332 14.095	±1/2	674.8	0.970 1.241 14.286	±1/2	663.4	0.802 0.885 14.427	±1/2	662.7	0.567 0.748 14.535	±1/2
7	874.9	0.133 0.220 17.131	±5/2	812.3	0.125 0.209 17.147	±5/2	800.4	0.118 0.195 17.178	±5/2	805.0	0.121 0.199 17.156	±5/2
8	1028.5	0.018 0.031 19.644	±1/2	967.9	0.023 0.041 19.603	±1/2	950.0	0.020 0.034 19.598	±1/2	954.5	0.027 0.049 19.587	±1/2

Table S23. Wave functions with definite projection of the total moment | m_J > for the lowest eight KDs of individual DyIII fragments for complexes **2**, **4** and **6**.

	E/cm^{-1}	wave functions
2(Dy1)	0.0	98.6%|±15/2>
	290.6	65.4%|±13/2>+19.2%|±9/2>+5.7%|±5/2>
	532.2	39.4%|±11/2>+29.9%|±7/2>+15.1%|±13/2>+8.5%|±3/2>
	656.1	31.0%|±5/2>+23.5%|±9/2>+18.7%|±11/2>+15.0%|±13/2>+8.1%|±1/2>
	708.3	36.2%|±3/2>+23.8%|±11/2>+16.9%|±9/2>+9.5%|±1/2>+9.4%|±7/2>
	760.0	41.3%|±1/2>+20.8%|±9/2>+19.7%|±7/2>+8.3%|±5/2>
	803.1	30.3%|±5/2>+25.1%|±7/2>+21.5%|±3/2>+13.1%|±9/2>
	903.9	31.1%|±1/2>+27.0%|±3/2>+20.2%|±5/2>+12.7%|±7/2>
4(Dy1)	0.0	98.0%|±15/2>
	287.9	49.5%|±13/2>+23.1%|±9/2>+8.6%|±5/2>+6.4%|±11/2>+5.1%|±7/2>
	524.7	31.7%|±11/2>+29.0%|±7/2>+25.6%|±13/2>+8.0%|±3/2>
	640.3	31.2%|±5/2>+19.7%|±11/2>+18.7%|±13/2>+17.8%|±9/2>+8.5%|±1/2>
	691.8	37.6%|±3/2>+24.1%|±11/2>+16.2%|±9/2>+9.9%|±1/2>+6.5%|±7/2>
	755.5	41.9%|±1/2>+20.4%|±9/2>+18.5%|±7/2>+7.5%|±11/2>+6.9%|±5/2>
	799.5	28.8%|±5/2>+25.3%|±7/2>+19.6%|±3/2>+14.7%|±9/2>+6.2%|±11/2>
	879.5	29.4%|±1/2>+26.2%|±3/2>+20.3%|±5/2>+13.5%|±7/2>
6_*a*(Dy1)	0.0	97.4%|±15/2>
	284.7	52.9%|±13/2>+24.8%|±9/2>+9.6%|±5/2>+3.9%|±1/2>
	513.2	32.9%|±11/2>+31.2%|±7/2>+18.2%|±13/2>+10.0%|±3/2>
	627.0	29.6%|±5/2>+21.4%|±13/2>+20.5%|±11/2>+14.3%|±9/2>+9.3%|±1/2>
	670.4	35.3%|±3/2>+24.3%|±11/2>+17.9%|±9/2>+9.6%|±1/2>+5.3%|±7/2>
	723.6	39.3%|±1/2>+20.7%|±9/2>+19.4%|±7/2>+8.7%|±11/2>+6.3%|±5/2>
	775.7	28.8%|±5/2>+24.9%|±7/2>+19.4%|±3/2>+14.8%|±9/2>+6.4%|±11/2>
	922.5	29.6%|±1/2>+26.2%|±3/2>+20.0%|±5/2>+13.3%|±7/2>+7.1%|±9/2>
6_*b*(Dy1)	0.0	97.3%|±15/2>
	299.3	46.8%|±13/2>+23.1%|±9/2>+9.3%|±11/2>+8.1%|±5/2>+5.8%|±7/2>
	550.6	29.3%|±7/2>+28.8%|±11/2>+25.6%|±13/2>+9.5%|±3/2>
	679.5	32.2%|±5/2>+20.6%|±13/2>+16.3%|±9/2>+14.9%|±11/2>+11.6%|±1/2>
	724.7	35.7%|±3/2>+26.4%|±11/2>+15.2%|±9/2>+10.7%|±1/2>+5.1%|±7/2>
	778.6	37.5%|±1/2>+22.5%|±9/2>+18.6%|±7/2>+9.5%|±11/2>+6.3%|±5/2>
	839.3	28.5%|±5/2>+26.0%|±7/2>+18.9%|±3/2>+15.3%|±9/2>+6.4%|±11/2>
	895.1	30.5%|±1/2>+26.4%|±3/2>+20.1%|±5/2>+12.9%|±7/2>

Table S24. Fitted exchange couplings $\tilde{J}$exch, the calculated dipole-dipole interactions $\tilde{J}$dip and the total constants $\tilde{J}$total between magnetic center ions in **2**, **4** and **6** (cm^{-1}) The intermolecular interactions zJ′ of **2**, **4** and **6** were fitted to –0.04, –0.07, –0.03 and –0.03 cm^{-1}, respectively.

	2	**4**	**6_*a***	**6_*b***
$\tilde{J}_{dip}$	5.66	5.70	5.76	5.63
$\tilde{J}_{exch}$	–6.00	–7.50	–7.50	–7.50
$\tilde{J}_{total}$	–0.34	–1.80	–1.74	–1.87

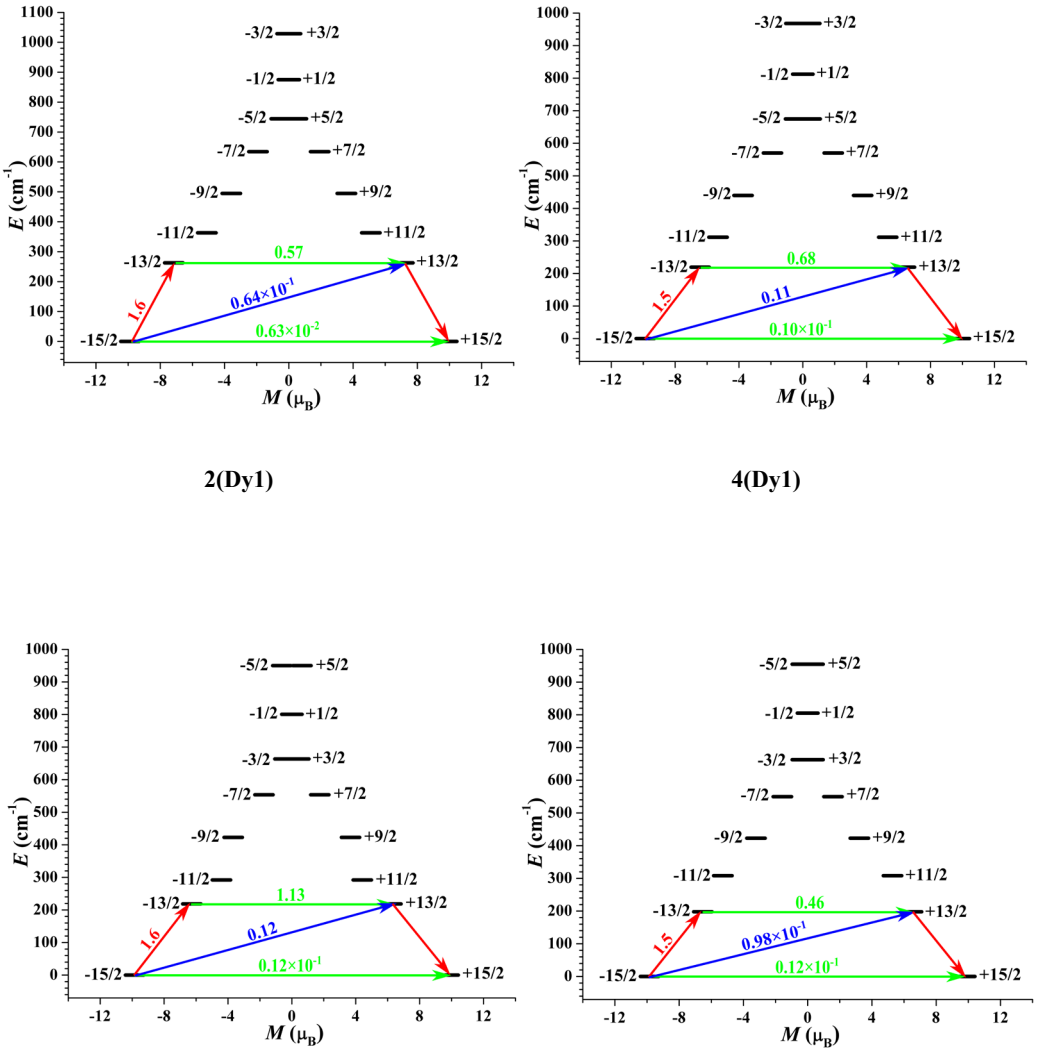

Fig. S62 Magnetization blocking barriers of individual Dy^{III} fragments for **2**, **4** and **6**. The thick black lines represent the KDs as a function of their magnetic moment along the magnetic axis. The green lines correspond to diagonal quantum tunneling of magnetization (QTM); the blue line represent off-diagonal relaxation process. The numbers at each arrow stand for the mean absolute value of the corresponding matrix element of transition magnetic moment.

To fit the exchange interactions in complexes **2**, **4** and **6**, we took two steps to obtain it. Firstly, we calculated individual Dy^{III} fragments using CASSCF/RASSI-SO to obtain the corresponding magnetic properties. Then, the exchange interaction between the magnetic centers was considered within the Lines model,[S5] while the account of the dipole-dipole magnetic coupling was treated exactly. The Lines model is effective and has been successfully used widely in the research field of *d* and *f*-elements single-molecule magnets.[S6–S7]

For complexes **2**, **4** and **6**, there is only one type of $\tilde{J}$. The Ising exchange Hamiltonian is:

$$\hat{H}_{exch} = -\tilde{J}\hat{\tilde{S}}_{Dy1}\hat{\tilde{S}}_{Dy1'}$$

$\tilde{J} = 25\cos\varphi J$, where φ is the angle between the anisotropy axes on two Dy^{III} sites, and *J* is the Lines exchange coupling parameter. $\tilde{S}_{Dy}$ = 1/2 is the ground pseudospin on the Dy^{III} site. $\tilde{J}_{total}$ is the parameter of the total magnetic interaction ($\tilde{J}_{total} = \tilde{J}_{dip} + \tilde{J}_{exch}$) between magnetic center ions. The dipolar magnetic coupling can be calculated exactly, while the exchange coupling constant was fitted through comparison of the computed and measured magnetic susceptibilities using POLY_ANISO program.[S2–S4]

Table S25. Exchange energies *E* (cm^{-1}), the energy difference between each exchange doublets Δ_t (cm^{-1}) and the main values of the g_z for the lowest two exchange doublets of **2**, **4** and **6**.

	2			**4**		
	E	Δ_t	g_z	*E*	Δ_t	g_z
1	0.00000000	0.909×10^{-5}	0.000	0.00000000	0.276×10^{-4}	0.000
	0.00000909			0.00002757		
2	0.02462557	0.378×10^{-5}	39.556	0.70432392	0.130×10^{-4}	39.483
	0.02462935			0.70433689		
	6_*a*			**6_*b***		
	E	Δ_t	g_z	*E*	Δ_t	g_z
1	0.00000000	0.397×10^{-4}	0.000	0.00000000	0.367×10^{-4}	0.000
	0.00003973			0.00003673		
2	0.66226579	0.194×10^{-4}	39.402	0.71914311	0.183×10^{-4}	39.363
	0.66228523			0.71916136		

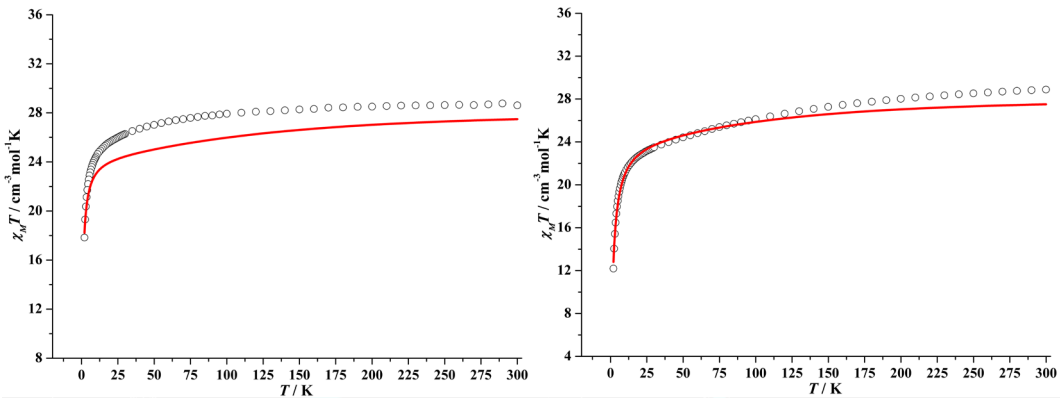

2 **4**

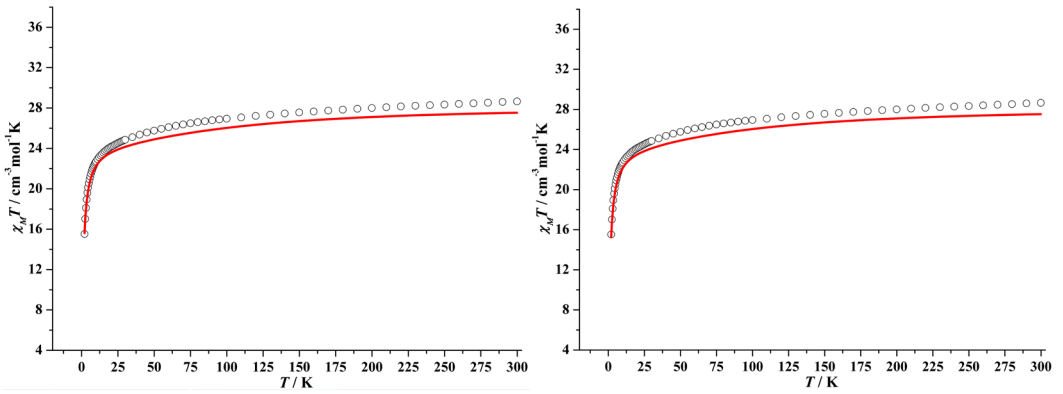

6_*a* **6_*b***

Fig. S63 Calculated (red solid line) and experimental (black square dot) data of magnetic susceptibilities of **2**, **4**，**6**. The intermolecular interactions *zJ′* of complexes **2**, **4** and **6** were fitted to –0.04, –0.07, –0.03 and –0.03 cm^{-1}, respectively.

References:

S1 Aquilante, F.; Autschbach, J.; Carlson, R. K.; Chibotaru, L. F.; Delcey, M. G.; De Vico, L.; Galván, I. F.; Ferré, N.; Frutos, L. M.; Gagliardi, L.; Garavelli, M.; Giussani, A.; Hoyer, C. E.; Li Manni, G.; Lischka, H.; Ma, D.; Malmqvist, P. Å.; Müller, T.; Nenov, A.; Olivucci, M.; Pedersen, T. B.; Peng, D.; Plasser, F.; Pritchard, B.; Reiher, M.; Rivalta, I.; Schapiro, I.; Segarra-Martí, J.; Stenrup, M.; Truhlar, D. G.; Ungur, L.; Valentini, A.; Vancoillie, S.; Veryazov, V.; Vysotskiy, V. P.; Weingart, O.; Zapata, F.; Lindh, R. *J. Comput. Chem.* **2016**, *37*, 506−541.

S2 Chibotaru, L. F.; Ungur, L.; Soncini, A. *Angew. Chem., Int. Ed.* **2008**, *47*, 4126–4129.

S3 Ungur, L.; Van den Heuvel, W.; Chibotaru, L. F. *New J. Chem.* **2009**, *33*, 1224–1230.

S4 Chibotaru, L. F.; Ungur, L.; Aronica, C.; Elmoll, H.; Pilet, G.; Luneau, D. *J. Am. Chem. Soc.* **2008**, *130*, 12445–12455.

S5 Lines, M. E. *J. Chem. Phys*. **1971**, *55*, 2977–2984.

S6 Mondal, K. C.; Sundt, A.; Lan, Y. H.; Kostakis, G. E.; Waldmann, O.; Ungur, L.; Chibotaru, L. F.; Anson, C. E.; Powell, A. K. *Angew. Chem., Int. Ed*. **2012**, *51*, 7550–7554.

S7 Langley, S. K.; Wielechowski, D. P.; Vieru, V.; Chilton, N. F.; Moubaraki, B.; Abrahams, B. F.; Chibotaru, L. F.; Murray, K. S. *Angew. Chem., Int. Ed*. **2013**, *52*, 12014–12019.